assessed by computer-based planimetry of Masson's trichrome-stained heart tissue, was significantly smaller in the Sheet group than in the Sham group (Figure 5C).

Vascular density, assessed by immunohistochemistry for vWF, in both the endocardium and epicardium, tended to be greater in the infarct and border areas than in the remote area of sham-operated hearts. In addition, vascular density in the endocardium was significantly greater than that in the epicardium in the border area post-sham operation, whereas vascular density did not differ significantly between the subendocardium and subepicardium in either the infarct or remote area of the sham-operated hearts. After cell-sheet implantation, vascular density did not differ between the subendocardium and subepicardium in either the infarct or remote area, but it was significantly greater in the subendocardium than in the subepicardium in the border region in the Sheet group. Only vascular density in the subendocardium of the border zone showed a significant difference between the sheet-implanted and sham-operated hearts (Figures 5D,E).

Profiles of Expression of Reverse LV Remodeling-Related Molecules

A variety of molecules that are expressed intramyocardial and potentially related to reverse LV remodeling were assessed by real-time PCR. Relative expression of VEGF was significantly increased in the Sheet group compared with the Sham group, whereas other factors, such as TNF-α, IL-6, bFGF and IGF-1, did not show any significant differences (Figure 6). Relative expression of BNP was significantly smaller post-cell-sheet implantation than post-sham operation.

Discussion

In the present study, SMB cell-sheet implantation produced the following major effects: (1) progression of LV remodeling was prevented and global LVEF decreased; (2) subendocardial strain was significantly greater than subepicardial strain in the treated border region; (3) vascular density in the subendocardium was significantly higher than in the subepicardium of the treated region; and (4) the expression of VEGF was significantly increased. Our data therefore suggest that SMB cell-sheet implantation enhanced the paracrine effect (eg, VEGF), inducing angiogenesis and thus improving regional myocardial performance in the targeted area, and these effects were more significant in the subendocardium than in the subepicardium of the border lesion.

The mechanism of restoration of damaged myocardium by SMB cell-sheet implantation is complex and many pathways are involved in the recovery of treated myocardium.[5–7,20,21] Recent reports have described the beneficial results of SMB cell-sheet implantation in several animal experimental models and patients with heart failure, which were primarily attributed to the following factors: the secretion of cytokines from the implanted cell-sheets (ie, paracrine effect), including angiogenic growth factors, the formation of capillary networks, and finally, mechanical inhibition of LV dilatation by implantation of cell-sheets.[1,3,5–10] Previous studies supported this and have shown that SMB and bone marrow-derived mesenchymal stem cell sheets secrete growth factors (eg, VEGF) into the myocardium, and that these factors accelerate neovascularization in the damaged area.[5–10] Among the many complex molecular and cellular mechanisms, the role of VEGF and its signaling pathway has been intensively investigated in vivo.[22] Toyota et al reported that the expression of VEGF is critical to the growth of coronary collateral vessels.[23] In the present study, VEGF expression was significantly increased in the Sheet group compared with the Sham group, suggesting that SMB cell-sheet implantation induced an angiogenic response via VEGF. Although many studies have proved that released cytokines from implanted cells play a major role in generating therapeutic effects on ischemic myocardium, there is currently no modality to precisely evaluate the section of damaged myocardium affected by released cytokines.

For tissue engineering as cardiac therapy, the creation of mature and functional vessels as neo-vascularization is essential. It has been reported that capillary formation occurs via 2 basic vessel-constructing processes: angiogenesis (ie, the formation of new capillaries via sprouting or intussusception from preexisting vessels), and vasculogenesis.[24] It has been also reported that angiogenesis requires dynamic temporal and spatial regulated interaction among endothelial cells, pericytes, and angiogenic factors.[25] Together with the morphology of vessels forming within myocardial tissues, including the diameter and stability of the vessel walls, we propose another possible mechanism that vessel maturation may occur under pathological stimuli such as increased blood perfusion in the in vivo environment.

To separately elucidate the effects of SMB cell-sheet implantation on LV regional function in the treated infarcted and border areas, we used tissue Doppler derived strain and the corresponding analysis software. SMB cell-sheet implantation therapy induced an improvement in regional myocardial performance in the treated border area, but not the treated infarcted area. Moreover, we speculate that regional functional recovery may correlate well with our data for the upregulation of VEGF gene expression and significant angiogenesis in the border region of the ischemic/infarcted myocardium. In addition, on the basis of the results of an improvement in the strain value as determined by tissue Doppler derived strain, the model used in the present study can be considered as the hibernating state, especially in the border region, instead of as a model of chronic MI.[15] Taken together, the results suggest that SMB cell-sheet therapy may rescue potentially salvageable myocardium partially by reperfusion, thus improving myocardial performance. Together with the paracrine effects of the implanted SMB cell-sheet, humoral substances might have a beneficial effect on native cardiomyocytes and viable surrounding muscle cells, leading to the prevention of global myocardial remodeling.[15] Our results may support the concept of a molecular mechanism of paracrine effect associated with cardioprotective factors released following SMB cell-sheet implantation.

The TMSP showed that SMB cell-sheet implantation induced a more significant regional recovery in the subendocardium than in the subepicardium, despite the SMB cell-sheet being implanted on the epicardium. To understand this mechanism in more detail, we performed tissue strain imaging and the results reflect the fundamental differences in functional properties within the LV myocardium. Ischemic injury did not occur in a uniform manner throughout the LV myocardium. Regional differences in metabolism and energy requirements render the endocardium more vulnerable to injury. Myocardial injury and stunning therefore usually originate in the endocardium and, with time, progress to include the epicardium.[26] In general, VEGF expression is activated under hypoxic conditions, a reasonable mechanism for holding oxygen tension constant.[27] Some previous investigators suggested that a soluble VEGF receptor (ie, sVEGFR1) increases in response to hypoxia.[28,29] It seems reasonable to assume that paracrine signaling between VEGF and sVEGFR1 might be evoked predominantly

in the ischemic region to regulate angiogenesis, and improve regional myocardial performance, in the face of hypoxia. Thus, the conceptual approach of SMB cell-sheet implantation is the eliciting of a cardiac protective response (eg, angiogenesis and microcirculation) during ischemia and prevention of the progression of ischemic injury and tissue necrosis. A possible mechanism to explain our results is that SMB cell-sheet implantation induces the release of cytokines and enhances the development of microvasculature (ie, microcirculation) that might be particularly vulnerable to injury during ischemia, and upon reperfusion, enhances the recovery of myocardial performance.[30] There is currently an emerging theory that the microcirculation could be the primary target for the amelioration of the potentially devastating consequences of ischemic injury. Nevertheless, it remains to be determined whether the primary benefits of SMB cell-sheet implantation are a consequence of (1) a cardioprotective effect by contributing directly to cardiomyocyte regeneration, (2) paracrine effects emanating from the SMB cell-sheet, or (3) a combination of these effects. Also, it is unclear whether the source of the therapeutic cytokines (eg, VEGF) is the implanted cells or native cardiac cells, such as ischemic cardiomyocytes, endothelial cells, or resident macrophages.

Study Limitations

Considerable caution must be exercised in extrapolating the present results. We did not validate myocardial strain values using other methods (eg, sonomicrometry). However, sonomicrometry is not always suitable for the assessment of transmural distribution of myocardial strain. We believe that our measurements were accurate because the displacement data obtained by our method were shown to be accurate.[31]

TDI is generally recognized as a 1D method and can measure myocardial deformation along the beam direction only. TDI-based strain estimation suffers from decorrelation caused by both axial motion and motion transverse to the beam direction. 2D speckle tracking strain imaging was introduced to overcome these limitations to myocardial imaging by estimating the 2D in-plane displacements with moderate frame rates.[32] These 2 methods are very different in principle and detail, directly affecting estimation accuracy, even of the same parameters. These differences must be noted when parameters from either method are applied clinically to myocardial contractility characterization. Moreover, the operator must avoid myocardium with large transverse motion to minimize the effect of transverse motion on TDI measurements.

Several investigators have suggested that a zone of dysfunctional myocardium caused by coronary artery occlusion might exist at the border of an infarct, with graded hypoperfusion extending out from the central region of infarction.[33,34] Subsequent reports demonstrated that coronary microvessels function essentially as end vessels with sharp boundaries between adjacent vascular beds, but that intermediate levels of mean blood flow can exist as a result of admixture of peninsulas of ischemic tissue intermingled with regions of normally perfused myocardium.[35–39] Although there is tremendous variability in the coronary artery blood supply to myocardial segments, it was believed to be appropriate to assign individual segments to specific coronary artery territories.

Conclusions

In conclusion, assessment of the TMSP enabled precise evaluation of the effect of cell-sheet implantation on layer-specific myocardial function. Autologous SMB cell-sheet implantation enhanced the paracrine effect, induced angiogenesis, and increased blood perfusion, thus improving regional myocardial performance more effectively in the subendocardium as compared with the subepicardium of the treated border zone area.

Sources of Funding

The present study was supported by Grants for the Research and Development of the Myocardial Regeneration Medicine Program from the New Energy Industrial Technology Development Organization (NEDO), Japan.

Acknowledgments

We thank Mr Shigeru Matsumi and Mrs Masako Yokoyama for their excellent technical assistance.

Disclosure

There is no conflict of interest related to this article.

References

1. Menasche P, Hagege AA, Scorsin M, Pouzet B, Desnos M, Duboc D, et al. Myoblast transplantation in heart failure. *Lancet* 2001; **357:** 279–280.
2. Ghostine S, Carrion C, Souza LC, Richard P, Bruneval P, Vilquin JT, et al. Long-term efficacy of myoblast transplantation on regional structure and function after myocardial infarction. *Circulation* 2002; **106:** I131–I136.
3. Hagege AA, Marolleau JP, Vilqiun JT, Alheritiere A, Peyrard S, Duboc D, et al. Skeletal myoblast transplantation in ischemic heart failure: Long-term follow-up of the first phase I cohort of patients. *Circulation* 2006; **114:** I108–I113.
4. Menasche P, Hagege AA, Vilquin JT, Desnos M, Abergel E, Pouzet B, et al. Autologous skeletal myoblast transplantation for severe postinfarction left ventricular dysfunction. *J Am Coll Cardiol* 2003; **41:** 1078–1083.
5. Miyagawa S, Saito A, Sakaguchi T, Yoshikawa Y, Yamauchi T, Imanishi Y, et al. Impaired myocardium regeneration with skeletal cell sheets: A preclinical trial for tissue-engineered regeneration therapy. *Transplantation* 2010; **90:** 364–372.
6. Miyagawa S, Sawa Y, Sakakida S, Taketani S, Kondoh H, Memon IA, et al. Tissue cardiomyoplasty using bioengineered contractile cardiomyocyte sheets to repair damaged myocardium: Their integration with recipient myocardium. *Transplantation* 2005; **80:** 1586–1595.
7. Memon IA, Sawa Y, Fukushima N, Matsumiya G, Miyagawa S, Taketani S, et al. Repair of impaired myocardium by means of implantation of engineered autologous myoblast sheets. *J Thorac Cardiovasc Surg* 2009; **130:** 646–653.
8. Sekiya N, Matsumiya G, Miyagawa S, Saito A, Shimizu T, Okano T, et al. Layered implantation of myoblast sheets attenuates adverse cardiac remodeling of the infarcted heart. *J Thorac Cardiovasc Surg* 2009; **138:** 985–993.
9. Miyagawa S, Roth M, Saito A, Sawa Y, Kostin S. Tissue-engineered cardiac constructs for cardiac repair. *Ann Thorac Surg* 2011; **91:** 320–329.
10. Fujita T, Sakaguchi T, Miyagawa S, Saito A, Sekiya N, Izutani H, et al. Clinical impact of combined transplantation of autologous skeletal myoblasts and bone marrow mononuclear cells in patients with severely deteriorated ischemic cardiomyopathy. *Surg Today* 2011; **41:** 1029–1036.
11. Janseens S, Dubois C, Bogaert J, Theunissen K, Deroose C, Desmet W, et al. Autologous bone marrow-derived stem-cell transfer in patients with ST-segment elevation myocardial infarction: Double-blind, randomized controlled trial. *Lancet* 2006; **367:** 113–121.
12. Maruo T, Nakatani S, Jin Y, Uemura K, Sugimachi M, Ueda-Ishibashi H, et al. Evaluation of transmural distribution of viable muscle by myocardial strain profile and dobutamine stress echocardiography. *Am J Physiol Heart Circ Physiol* 2007; **292:** H921–H927.
13. Hasegawa T, Nakatani S, Kanzaki H, Abe H, Kitakaze M. Heterogeneous onset of myocardial relaxation in subendocardial and subepicardial layers assessed with tissue strain imaging: Comparison of normal and hypertrophied myocardium. *J Am Coll Cardiol Img* 2009; **2:** 701–708.
14. Tanimoto T, Imanishi T, Tanaka A, Yamano T, Kitabata H, Takarada S, et al. Bedside assessment of myocardial viability using transmural strain profile in patients with ST-elevation myocardial infarction: Comparison with cardiac magnetic resonance imaging. *J Am Soc Echocardiogr* 2009; **22:** 1015–1021.

15. Reimer KA, Jennings RB. The 'wavefront phenomenon' of myocardial ischemic death. II: Transmural progression of necrosis within the framework of ischemic bed size (myocardium at risk) and collateral flow. *Lab Invest* 1979; **40:** 633–644.
16. Teramoto N, Koshino K, Yokoyama I, Miyagawa S, Ose T, Zeniya T, et al. Experimental pig model of old myocardial infarction with long survival leading to chronic LV dysfunction and remodeling as evaluated by PET. *J Nucl Med* 2011; **52:** 761–768.
17. Sade LE, Severyn DA, Kanzaki H, Dohi K, Gorcsan J 3rd. Second-generation tissue Doppler with angle-corrected color-coed wall displacement for quantitative assessment of regional left ventricular function. *Am J Cardiol* 2003; **92:** 554–560.
18. Hu Q, Wang X, Lee J, Mansoor A, Liu J, Zeng L, et al. Profound bioenergetic abnormalities in peri-infarct myocardial regions. *Am J Physiol Heart Circ Physiol* 2006; **291:** H648–H657.
19. Horiguchi K, Sakakida-Kitagawa S, Sawa Y, Li ZZ, Fukushima N, Shirakura R, et al. Selective chemokine and receptor gene expressions in allografts that develop transplant vasculopathy. *J Heart Lung Transplant* 2002; **21:** 1090–1100.
20. Pagani FD, DerSimonian H, Zawadzka A, Wetzel K, Edge AS, Jacoby DB, et al. Autologous skeletal myoblasts transplanted to ischemia-damaged myocardium in humans: Histological analysis of cell survival and differentiation. *J Am Coll Cardiol* 2003; **41:** 1078–1083.
21. Suzuki K, Murtuza B, Fukushima S, Smolenski RT, Varela-Carver A, Coppen SR, et al. Targeted cell delivery into infarcted rat hearts by retrograde intracoronary infusion: Distribution, dynamics, and influence on cardiac function. *Circulation* 2004; **110:** II225–II230.
22. Toyota E, Matsunaga T, Chilian WM. Myocardial angiogenesis. *Mol Cell Biochem* 2004; **264:** 35–44.
23. Toyota E, Warltier DC, Brock T, Ritman E, Kolz C, O'Malley P, et al. Vascular endothelial growth factor is required for coronary collateral growth in the rat. *Circulation* 2005; **112:** 2108–2113.
24. Risau W. Mechanisms of angiogenesis. *Nature* 1997; **386:** 671–674.
25. Goumans MJ, Valdimarsdottir G, Itoh S, Rosendahl A, Sideras P, ten Dijke P. Balancing the activation state of the endothelium via two distinct TGF-beta type 1 receptors. *EMBO J* 2002; **21:** 1743–1753.
26. Zeng L, Hu Q, Wang X, Mansoor A, Lee J, Feygin J, et al. Bioenergetic and functional consequences of bone marrow-derived multipotent progenitor cell transplantation in hearts with postinfarction left ventricular remodeling. *Circulation* 2007; **115:** 1866–1875.
27. Shweiki D, Itin A, Soffer D, Keshet E. Vascular endothelial growth factor induced by hypoxia may mediate hypoxia-initiated angiogenesis. *Nature* 1992; **359:** 843–845.
28. Nagamatsu T, Fujii T, Kusumi M, Zou L, Yamashita T, Osuga Y, et al. Cytotrophoblasts up-regulate soluble fms-like tyrosine kinase-1 expression under reduce oxygen: An implication for the placental vascular development and the pathology of preeclampsia. *Endocrinology* 2004; **145:** 4838–4845.
29. Munaut C, Lorquet S, Pequeux C, Blacher S, Berndt S, Frankenne F, et al. Hypoxia is responsible for soluble vascular endothelial growth factor receptor-1 (VEGFR-1) but not for soluble endoglin induction in villous trophoblast. *Hum Reprod* 2008; **23:** 1407–1415.
30. Hearse DJ, Maxwell L, Saldanha C, Gravin JB. The myocardial vasculature during ischemia and reperfusion: A target for injury and protection. *J Mol Cell Cardiol* 1993; **25:** 759–800.
31. Panting JR, Gatehouse PD, Yang GZ, Grothues F, Firmin DN, Collins P, et al. Abnormal subendocardial perfusion in cardiac syndrome X detected by cardiovascular magnetic resonance imaging. *N Engl J Med* 2002; **346:** 1948–1953.
32. van Ramshorst J, Atsma DE, Beeres SL, Mollema SA, Ajmone Marsan N, Holman ER, et al. Effect of intramyocardial bone marrow cell injection of left ventricular dyssynchrony and global strain. *Heart* 2009; **95:** 119–124.
33. Buda AJ, Zotz RJ, Gallagher KP. Characterization of the functional border zone around regionally ischemic myocardium using circumferential flow-function maps. *J Am Coll Cardiol* 1986; **8:** 150–158.
34. Homans DC, Asinger R, Elsperger KJ, Erlien D, Sublette E, Mikell F, et al. Regional function and perfusion at the lateral border of ischemic myocardium. *Circulation* 1985; **71:** 1038–1047.
35. Patterson RE, Kirk ES. Analysis of coronary collateral structure, function, and ischemic border zones in pigs. *Am J Physiol Heart Circ Physiol* 1983; **244:** H23–H31.
36. Shudo Y, Matsumiya G, Takeda K, Matsue H, Taniguchi K, Sawa Y. Novel software package for quantifying local circumferential myocardial stress. *Int J Cardiol* 2011; **17:** 134–136.
37. Kainuma S, Taniguchi K, Toda K, Funatsu T, Kondoh H, Nishino M, et al. Restrictive mitral annuloplasty for functional mitral regurgitation. *Circ J* 2011; **75:** 571–579.
38. Takeda K, Matsumiya G, Hamada S, Sakaguchi T, Miyagawa S, Yamauchi T, et al. Left ventricular basal myocardial scarring detected by delayed enhancement magnetic resonance imaging predicts outcomes after surgical therapies for patients with ischemic mitral regurgitation and left ventricular dysfunction. *Circ J* 2011; **75:** 148–156.
39. Saito S, Matsumiya G, Sakaguchi T, Miyagawa S, Yoshikawa Y, Yamauchi T, et al. Risk factor analysis of long-term support with left ventricular assist system. *Circ J* 2010; **74:** 715–722.

Spatially Oriented, Temporally Sequential Smooth Muscle Cell-Endothelial Progenitor Cell Bi-Level Cell Sheet Neovascularizes Ischemic Myocardium

Yasuhiro Shudo, MD, FAHA; Jeffrey E. Cohen, MD; John W. MacArthur, MD; Pavan Atluri, MD, FAHA; Philip F. Hsiao, BA; Elaine C. Yang, MS; Alexander S. Fairman, BA; Alen Trubelja, BS; Jay Patel, BS; Shigeru Miyagawa, MD, PhD; Yoshiki Sawa, MD, PhD; Y. Joseph Woo, MD, FAHA

Background—Endothelial progenitor cells (EPCs) possess robust therapeutic angiogenic potential, yet may be limited in the capacity to develop into fully mature vasculature. This problem might be exacerbated by the absence of a neovascular foundation, namely pericytes, with simple EPC injection. We hypothesized that coculturing EPCs with smooth muscle cells (SMCs), components of the surrounding vascular wall, in a cell sheet will mimic the native spatial orientation and interaction between EPCs and SMCs to create a supratherapeutic angiogenic construct in a model of ischemic cardiomyopathy.

Methods and Results—Primary EPCs and SMCs were isolated from Wistar rats. Confluent SMCs topped with confluent EPCs were spontaneously detached from the Upcell dish to create an SMC-EPC bi-level cell sheet. A rodent ischemic cardiomyopathy model was created by ligating the left anterior descending coronary artery. Rats were then immediately divided into 3 groups: cell-sheet transplantation (n=14), cell injection (n=12), and no treatment (n=13). Cocultured EPCs and SMCs stimulated an abundant release of multiple cytokines in vitro. Increased capillary density and improved blood perfusion in the borderzone elucidated the significant in vivo angiogenic potential of this technology. Most interestingly, however, cell fate–tracking experiments demonstrated that the cell-sheet EPCs and SMCs directly migrated into the myocardium and differentiated into elements of newly formed functional vasculature. The robust angiogenic effect of this cell sheet translated to enhanced ventricular function as demonstrated by echocardiography.

Conclusions—Spatially arranged EPC-SMC bi-level cell-sheet technology facilitated the natural interaction between EPCs and SMCs, thereby creating structurally mature, functional microvasculature in a rodent ischemic cardiomyopathy model, leading to improved myocardial function. (***Circulation*. 2013;128[suppl 1]:S59–S68.**)

Key Words: angiogenesis ■ cardiovascular diseases ■ cells ■ endothelium ■ heart failure ■ tissue

Heart failure is the leading cause of death in the United States, with a 5-year mortality of 50%. Current treatment for heart failure entails medical optimization, along with limited revascularization and reconstructive techniques. These interventions do not address the microvascular deficiencies that develop in ischemic cardiomyopathy (ICM). Myocardial regenerative and cellular therapy is attracting growing interest as a means to improve left ventricular (LV) function in advanced heart failure. Among the many candidate cells, endothelial progenitor cells (EPCs), the precursor of blood vessels, have demonstrated excellent potential for therapeutic angiogenesis. Recent reports show beneficial effects of EPC transplantation therapy in several animal experimental models and patients with heart failure.[1–3]

The mechanism by which damaged myocardium is restored by transplanted EPCs is complex and involves many pathways. Recent large-scale clinical trials, in which EPCs were delivered using direct myocardial injection[4] or catheter-based intracoronary procedures,[5,6] reported only modest therapeutic benefits. The limited benefits are at least partially because of poor localized cell survival after transplantation, thereby greatly attenuating the angiogenic potential of EPC therapy. In addition, mature vasculature requires the presence of supporting elements, such as smooth muscle cells (SMCs), which are not delivered with simple EPC injection. In contrast, cell-sheet technology delivers cells more effectively with minimal cell dispersion and myocardial injury and improves microvascular structure, leading to better cardiac function than that attained

From the Division of Cardiovascular Surgery, Department of Surgery, University of Pennsylvania School of Medicine, Philadelphia, PA (Y.S., J.E.C., J.W.M., P.A., P.F.H., E.C.Y., A.S.F., A.T., J.P., Y.J.W.); and Department of Cardiovascular Surgery, Osaka University Graduate School of Medicine, Osaka, Japan (S.M., Y.S.).

Presented at the American Heart Association meeting in Los Angeles, CA, November 3–7, 2012.

This article was handled independently by Frank Sellke, MD, as a Guest Editor.

Correspondence to Y. Joseph Woo, MD, Division of Cardiovascular Surgery, Department of Surgery, University of Pennsylvania School of Medicine, 3400 Spruce St, 6 Silverstein, Philadelphia, PA 19104. E-mail wooy@uphs.upenn.edu

© 2013 American Heart Association, Inc.

Circulation is available at http://circ.ahajournals.org DOI: 10.1161/CIRCULATIONAHA.112.000293

Downloaded from http://circ.ahajournals.org/ at Osaka University on May 20, 2014

by intracoronary injection or needle injection.[7–11] Specifically, the cell-sheet technology enables the construction of a cellular system that mimics the natural architecture of a desired tissue. Here, the proposed angiogenic therapy uses the cell sheet to optimize the spatial arrangement of EPCs and SMCs to maximally induce structurally mature vasculature. The cell sheet is generated on and removed from special dishes that are grafted with a temperature-responsive polymer that changes from hydrophobic to hydrophilic when the temperature is lowered. The greatest advantage of this technique is that the cell sheet consists of densely adherent cells without requiring an artificial scaffold, it is easily manipulated and has a high ability to integrate with native tissues without destroying the cell–cell or cell–extracellular matrix (ECM) adhesions in the cell sheet.[7] In addition, we focused on the concept that the natural endothelial–pericyte spatial relationship and interaction are crucial for vessel maturation and stabilization. Thus, we hypothesized that SMCs, which are components of vascular pericytes, would enhance EPC-mediated angiogenesis and facilitate blood vessel maturation. Neoangiogenesis should yield increased blood perfusion and restoration of cardiomyocyte viability. To demonstrate clear and direct contribution of the cell-sheet EPCs and SMCs to neovasculature, we constructed multiple fate-tracking experiments. A labeled cell sheet was created with EPCs from female rats ubiquitously expressing the enhanced green fluorescent protein (GFP), along with SMCs from male rats. This cell sheet with trackable elements was then implanted in female rats.

In short, this study examined the functional benefits of transplanting the bi-level cell sheet created from cocultured EPCs and SMCs in an ICM model, compared with direct myocardial needle injection.

Methods

Isolation of EPCs and SMCs

Wistar rats were administered pentobarbital (100 mg/kg, IP), and then the carotid artery was dissected and transected. Bone marrow mononuclear cells were isolated from the long bones of rats by density gradient centrifugation with Histopaque 1083 (Sigma-Aldrich) and cultured in endothelial basal medium-2 supplemented with EGM-2 SingleQuot (Lonza) containing human epidermal growth factor, 5% fetal bovine serum (Sigma-Aldrich), vascular endothelial growth factor (VEGF), basic human fibroblast growth factor, recombinant human long R3 insulin-like growth factor-1, ascorbic acid, gentamicin, and amphotericin B. The combination of endothelium-specific media and the removal of nonadherent bone marrow mononuclear cells were intended to select for the EPC phenotype. EPCs were cultured for 7 days in the same medium.[2] For EPC fate tracking, we used GFP transgenic female Wistar rats.

SMCs were isolated from the thoracic aorta of wild-type male Wister rats (3 weeks old; Charles River) by primary explant technique[12] and cultured in DMEM with 20% fetal bovine serum, gentamicin, and amphotericin B to confluency for 7 days at 37°C and 5% CO_2. For SMC fate tracking, we used male Wistar rats.

Bi-Level Cell-Sheet Preparation

The SMCs were plated at 1.5×10^5/cm^2 in a 35-mm Upcell dish, which is grafted with temperature-responsive polymers (CellSeed, Tokyo, Japan), and then cultured in EPC-specific medium. After 24 hours of culture at 37°C and 5% CO_2, EPCs were added at 1.5×10^5/cm^2 onto the Upcell dish, which was already confluent with SMCs. After 24 additional hours in culture, the dishes were transferred to another incubator, set at 20°C, for 1 hour to release the cultured cells as an intact cell sheet. Under this protocol, confluent SMCs topped with confluent EPCs were spontaneously detached from the plate as a sequentially cocultured and specifically spatially oriented SMC-EPC bi-level cell sheet (Figure 1A).[10,11]

Production and Release of Cytokines/Chemokines

To demonstrate proangiogenic biological activity, supernatant of the cocultured cells (EPCs: 1.5×10^5/cm^2, SMCs: 1.5×10^5/cm^2), EPCs (3.0×10^5/cm^2), or SMCs (3.0×10^5/cm^2), after being cultured for 24 hours, was centrifuged to remove debris and contaminating cells. Levels of VEGF, hepatocyte growth factor (HGF), transforming growth factor-β (TGFβ), and stromal cell–derived factor 1α (SDF1α) in the culture supernatants were analyzed by ELISA kit (Quantikine, R&D Minneapolis, MN; n=6 in each). ELISA was performed in duplicate.

Assessment of Cytokine Receptor Expressions by Flow Cytometry

To elucidate the biological impact of cocultured EPCs and SMCs on fetal liver kinase 1 (FLK1) and VEGF receptor 2 (VEGFR2) expression, flow cytometry was used in the EPC or SMC cultured with SMC or EPC using the transwell inserts, supplemented with recombinant VEGF, or media only for 24 hours (n=5 in each). The amount of VEGF was determined based on the results of ELISA. Test samples were incubated for 1 hour at room temperature with either mouse monoclonal anti-FLK1 (Santa Cruz Biotechnology) or rabbit anti-VEGFR2 (Abcam). After washing with cold fluorescence-activated cell sorter buffer, cells were incubated at room temperature

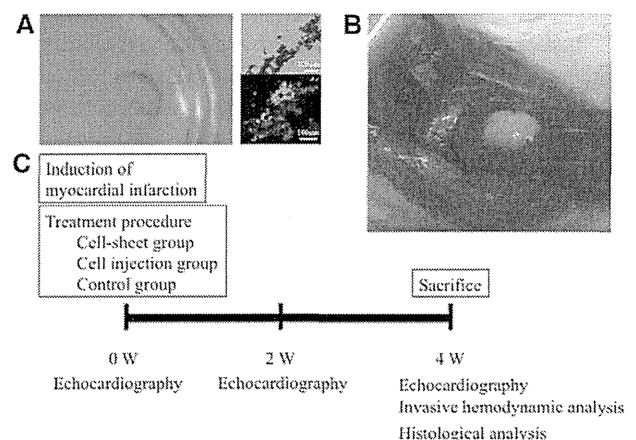

Figure 1. Preparation and transplantation of bi-level cocultured cell-sheet containing both endothelial progenitor cells (EPCs) and smooth muscle cells (SMCs). **A**, Confluent SMCs topped with confluent EPCs were spontaneously detached from an Upcell dish, which is grafted with temperature-responsive polymers (CellSeed, Tokyo, Japan), as a sequentially cocultured and specifically spatially oriented SMC-EPC bi-level cocultured cell-sheet. Hematoxylin-eosin staining; cross-sectional views of cell-sheet in vitro. Cocultured bi-level cell sheet maintained green fluorescent protein (GFP)-positive EPCs and Y chromosome–positive SMCs in separate layers in vitro. Red indicates rat Y *chromosome; green, GFP.* **B**, *Bi-level cocultured cell-sheet,* which consisted of 1.3×10^6 EPCs and 1.3×10^6 SMCs, was placed into the epicardium of the left ventricle covering the ischemic area. **C**, Study protocol used for assessment of cardiac function and histology. Wistar rats underwent induction of myocardial infarction by occluding the LAD permanently, followed by the concurrent treatment procedure. Cardiac function was assessed by echocardiography just before and at 2 and 4 weeks after the treatment procedure. Four weeks after the treatment procedure, invasive hemodynamic analysis and histological examination were performed after euthanasia.

Downloaded from http://circ.ahajournals.org/ at Osaka University on May 20, 2014

for 30 minutes with Alexa 647 chicken anti-mouse IgG (Invitrogen) and Alexa 488 donkey anti-rabbit IgG (Invitrogen). The percentage of cells expressing each cell surface antigen was analyzed with a Becton Dickinson FACSCalibur flow cytometer. Data analysis was performed using FlowJo 8.8.3 (Tree Star Inc).[3,13]

Rat ICM Model and Cell-Sheet Transplantation

Female Wistar rats (8 weeks old, 250–300g; Charles River) were anesthetized with ketamine (75 mg/kg IP) and xylazine (7.5 mg/kg IP), intubated in an endotracheal manner with a 19-gauge catheter, and mechanically ventilated (Hallowell EMC). Anesthesia was maintained by inhalation of 2.0% isoflurane (Clipper Distributing Company Llc, Saint Joseph, MO).

The proximal left anterior descending coronary artery (LAD) of Wistar rats was permanently occluded using a left thoracotomy approach. This produced a consistent and reproducible myocardial infarction encompassing 35% to 40% of the left ventricle.[1–3] Within 5 minutes after LAD ligation, the rats were allocated into 3 groups by simple randomization, considering that there were no differences among the animals at this time point: those that underwent cocultured cell-sheet transplantation (cell-sheet group, n=14), those that underwent cocultured cell injection (cell injection group, n=12), and those that underwent no intervention (control group, n=13). The rats were allowed to recover under care.

In the cell-sheet group, the cocultured bi-level cell sheet, which consists of 1.3×10^6 EPCs and 1.3×10^6 SMCs, was placed on the epicardium covering the ischemic area (Figure 1B). The cell injection group received 1.3×10^6 EPCs and 1.3×10^6 SMCs, diluted in saline for a total volume of 200 μL by direct intramyocardial injection with a 30-gauge needle. Each rat received the same number of cells. Animals were then kept in temperature-controlled individual cages for 4 weeks.

The rats were euthanized at 4 weeks after surgery by intravenous injection of 200 mg/kg of pentobarbital and 2 mEq/kg of potassium chloride, under terminal anesthesia, and the heart was excised.

Histological and Immunohistochemical Analyses

Four weeks after treatment, the hearts were dissected and embedded in optimum cutting temperature compound for 10-μm-thick cryosections. The cryosections were used for routine hematoxylin-eosin staining to assess the myocardial structure. Masson trichrome staining was performed to assess cardiac fibrosis in the peri-infarct borderzone. The fibrotic region was calculated as the percentage of myocardial area. The data were collected from 5 individual views per heart at a magnification of ×200. The heart cryosections were also stained with an antibody to von Willebrand factor (vWF; 1:200 dilution; Abcam) to assess capillary density, which was calculated as the number of positively stained capillary vessels in 5 randomly selected fields in the peri-infarct borderzone area, per heart. The cryosections were also stained with an antibody to proliferating cell nuclear antigen (1:200 dilution; Abcam) to assess cellular proliferative activity in 5 randomly selected fields in the peri-infarct borderzone area. The cryosections were also stained with an antibody to integrin β1 (1:100 dilution; Abcam) to estimate cell–matrix attachment in 5 randomly selected fields in the peri-infarct borderzone area. Cell nuclei were counterstained with 6-diamidino-2-phenylindole (Invitrogen). The images were examined by fluorescence microscopy (Leica). Image J software was used for quantitative morphometric analysis.

EPC-SMC Fate Tracking

The cell sheet, which consisted of EPCs from GFP transgenic female Wistar rats and SMCs from non-GFP male Wistar rats, was transplanted into the female Wistar rat heart. To detect the fate of EPCs, cryosections were stained with an anti-vWF antibody (1:1000 dilution; Abcam), anti-smooth muscle actin (SMA) antibody (1:1000 dilution; Abcam), anti-vascular endothelial-cadherin antibody (1:1000 dilution; Santa Cruz), and anti-GFP antibody (1:1000 dilution; Abcam). The secondary antibodies were Alexa Fluor 555 donkey anti-rabbit IgG (1:1000 dilution; Invitrogen) and Alexa Fluor 555 donkey anti-mouse IgG (1:1000 dilution; Invitrogen). To detect the fate of SMCs, fluorescence in situ hybridization was performed on cryosections, which were then stained with anti-SMA antibody (1:500 dilution; Abcam). The secondary antibody was Alexa Fluor 555 donkey anti-rabbit IgG (1:500 dilution; Invitrogen). Cell nuclei were counterstained with 6-diamidino-2-phenylindole. GFP-positive cells and rat Y chromosome–positive cells were counted, respectively, and corrected by total number of tissue cells to estimate the survival cells quantitatively. GFP- and vWF-positive cells were counted and corrected by total number of GFP-positive cells to examine vascular regeneration. Rat Y chromosome– and SMA-positive cells were counted and corrected by total number of rat Y chromosome–positive cells to examine vascular regeneration.

Myocardial Perfusion Analysis

To quantify myocardial perfusion, at 4 weeks after treatment 200 μg of fluorescein-labeled *Lycopersicon esculentum* (tomato) lectin (Vector Laboratories) was injected into the supradiaphragmatic inferior vena cava and allowed to circulate for 10 minutes. After lectin perfusion, the hearts were explanted and snap-frozen in liquid nitrogen. One-hundred twenty sequential images were obtained through 100-μm thick myocardial sections at the level of the papillary muscle using scanning laser confocal microscopy (z-series, ×20 air magnification, Zeiss LSM-510 Meta Confocal Microscope). Three-dimensional reconstructions of the image stacks were created using Velocity Software v.3.61 (Improvision). Fluorescein-labeled voxels were quantified as a percentage of total tissue section voxels, creating a quantifiable measurement of perfusion per unit of myocardial tissue volume.[2,3]

Echocardiographic Assessment

Echocardiography was performed under general anesthesia using 1.0% inhaled isoflurane just before and at 2 and 4 weeks after the treatment procedure (SONOS 7500, Philips Medical Systems, Andover, MA) with a 12-MHz transducer at an image depth of 2 cm (cell sheet, n=7; cell injection, n=8; control, n=9; Figure 1C). LV end-diastolic diameter (LVEDD), LV end-systolic diameter (LVESD), and end-diastolic anterior wall thickness at the level of the papillary muscles were measured for ≥3 consecutive cardiac cycles following the American Society for Echocardiology leading-edge method. Fractional shortening (FS) and ejection fraction (EF) were calculated as parameters of systolic function.[2,3,8] All analyses were performed by a single investigator in a group-blinded fashion.

Invasive Hemodynamic Assessment

Four weeks after the treatment procedure, animals (cell-sheet, n=6; cell injection, n=6; control, n=8) underwent invasive hemodynamic measurements with a pressure–volume conductance catheter (SPR-869; Millar Instruments, Inc; Figure 1C). The catheter was calibrated via 5-point cuvette linear interpolation with parallel conductance subtraction by the hypertonic saline method.[2,3] Rats were anesthetized using 1.0% inhaled isoflurane, and the catheter was introduced into the LV with a closed-chest approach via the right carotid artery. Measurements were obtained before and during inferior vena cava occlusion to produce static and dynamic pressure–volume loops under varying load conditions. Data were recorded and analyzed with LabChart version 6 software (AD Instruments) and ARIA Pressure Volume Analysis software (Millar Instruments, Inc). After hemodynamic assessment, the heart was removed for further histological analyses.

Statistical Analysis

Continuous variables are expressed as mean±SE. Comparisons between 2 groups were made using the Wilcoxon–Mann–Whitney *U* test because of small sample sizes. For comparisons among 3 groups, we used the Kruskal–Wallis test, followed by the post hoc pairwise Wilcoxon–Mann–Whitney *U* test. The multiplicity in pairwise comparisons was corrected by the Bonferroni procedure. A $P<0.05$ was

Downloaded from http://circ.ahajournals.org/ at Osaka University on May 20, 2014

considered statistically significant. All statistical calculations were performed using SPSS software (version 11.0; SPSS Inc, Chicago, IL) and JMP 9.0 (SAS Institute Inc, Cary, NC).

Animal Care and Biosafety

Wistar rats were obtained from Charles River. Food and water were provided ad libitum. This investigation conforms with the Guide for the Care and Use of Laboratory Animals published by the US National Institutes of Health (NIH Publication No. 85-23, revised 1996) and was approved by the Institutional Animal Care and Use Committee of the University of Pennsylvania (protocol 803394).

Results

Production and Release of Cytokines/Chemokines by Coculturing EPC With SMC

VEGF was significantly higher in the coculture supernatant than the SMC-only group and tended to be higher than the EPC-only group (Figure 2A). The secretion of HGF was remarkably enhanced in the coculture supernatant, whereas HGF levels were not evident in either the EPC- or SMC-alone group (Figure 2B). The concentration of TGFβ was significantly higher in the coculture supernatant than both the EPC- and SMC-only groups (Figure 2C). The secretion of SDF1α was remarkably higher in the cocultured group compared with EPC and SMC alone (Figure 2D).

Upregulated Expressions of FLK1 and VEGFR2 on Either EPC or SMC Under Cytokines-Rich Medium of SMC or EPC

Flow cytometric analysis demonstrated that the percentage of FLK1$^+$ EPCs and VEGFR2$^+$ EPCs in total EPC population was 1.3±0.3% and 3.2±0.8%, respectively. Supplementation with VEGF significantly increased the percentage of FLK1$^+$ EPCs (17.2±3.2%) and VEGFR2$^+$ EPCs (32.0±5.4%). Furthermore, the percentage of FLK1$^+$ and VEGFR2$^+$ EPCs was significantly greater after coculturing with SMC (FLK1$^+$, 39.6±9.2%; VEGFR2$^+$, 52.5±9.8%; Figure 3A and 3B).

Flow cytometric analysis demonstrated a statistically significant increase in the percentage of FLK1$^+$ SMCs cocultured with EPC compared with SMC alone (75.7±5.4 versus 23.9±2.5%; P=0.02). Addition of VEGF significantly increased FLK1$^+$ SMCs compared with SMC (Figure 3C and 3D). There was no significant difference in the VEGFR2$^+$ expression on SMCs (P=0.14, Kruskal–Wallis test).

Enhanced Capillary Density and Microvascular Perfusion After Cocultured Cell-Sheet Transplantation

A large number of vWF-positive blood vessels were detected in the peri-infarct borderzone myocardium after cell-sheet therapy compared with injection alone (Figure 4A). This demonstrated a superior enhancement of capillary density in the cell-sheet group (Figure 4B).

Similarly, lectin microangiography of the peri-infarct borderzone myocardium sections revealed a more densely and well-developed capillary network in the cell-sheet group compared with injection alone (Figure 4C). Quantitative analysis showed significantly enhanced perfusion in the peri-infarct borderzone myocardium in the cell-sheet group (Figure 4D).

Enhanced Cell Proliferation Activity After Cocultured Cell-Sheet Transplantation

A large number of proliferating cell nuclear antigen-positive cells were identified in the peri-infarct borderzone myocardium after cell-sheet therapy compared with control (Figure 4E and 4F).

Migration of EPCs and SMCs to Myocardium Contributing to Neovasculature

Cocultured bi-level cell sheet contained GFP-positive EPCs and Y chromosome–positive SMCs in separate layers in vitro (Figure 1A).

Four weeks after transplantation, the GFP-positive EPCs were detected in the myocardium at the transplanted site at an appropriate depth of 650 μm (Figure 4G). Immunostaining for vWF and GFP showed that transplanted EPCs were able to contribute to neovascularization of the host myocardium (Figure 4H). This was further supported by immunostaining for vascular endothelial-cadherin and GFP (Figure 4I). In addition, staining with antibody to SMA and GFP indicated that GFP-positive EPCs originating from the transplanted cocultured bi-level cell sheet migrated into the engineered

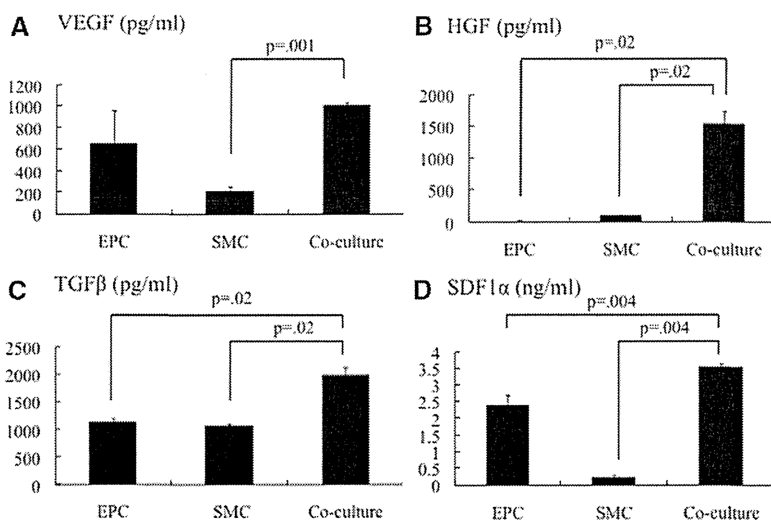

Figure 2. A, Vascular endothelial growth factor (VEGF), (**B**) hepatocyte growth factor (HGF), (**C**) transforming growth factor-β (TGFβ), and (**D**) stromal cell–derived factor 1α (SDF1α) in the culture supernatant, measured by ELISA. Cocultured endothelial progenitor cells (EPCs) with smooth muscle cells (SMCs) secreted abundant VEGF, HGF, TGFβ, and SDF1α compared with either EPC or SMC (n=6 in each; VEGF, P=0.002; HGF, P=0.01; TGFβ, P=0.01; SDF1α, P=0.001; Kruskal–Wallis test).

Downloaded from http://circ.ahajournals.org/ at Osaka University on May 20, 2014

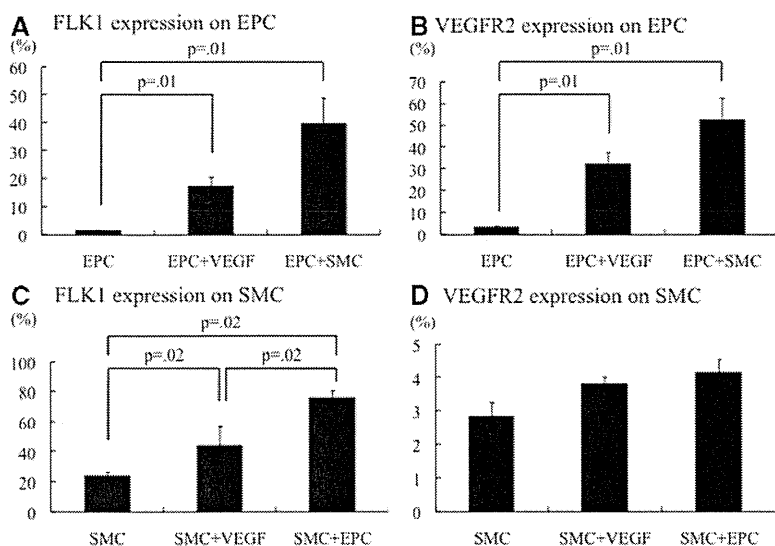

Figure 3. To elucidate the biological impact of cocultured endothelial progenitor cell (EPC)-smooth muscle cells (SMCs) on FLK1 and vascular endothelial growth factor receptor 2 (VEGFR2) expression, flow cytometry was used to study both EPC and SMC expression of these markers in the following settings: cocultured, cultured with VEGF, and cultured alone. The amount of VEGF used was determined based on the results of ELISA. **A** and **B**, The percentage of FLK1⁺ EPC and VEGFR2⁺ EPC was greatest in a cocultured setting (n=5 in each; FLK1 expression on EPC, P=0.01; VEGFR2 expression on EPC, P=0.01; Kruskal–Wallis test). **C** and **D**, Analysis of SMC FLK1⁺ expression demonstrated a significant increase in the cocultured group. There was no significant difference in the VEGFR2⁺ expression on SMC (n=4 in each; FLK1 expression on SMC, P=0.01; VEGFR2 expression on SMC, P=0.14; Kruskal–Wallis test).

myocardial tissues and were circumferentially surrounded by SMA-positive tissues (Figure 4J). Finally, to track SMCs from the cell sheet, we performed fluorescence in situ hybridization immediately to identify male SMCs in the female recipient. After the cell-sheet transplantation, GFP-positive EPCs and Y chromosome–positive SMCs were detected with a thickness of ≈50 μm into the epicardium (Figure 4K). Rat Y chromosome SMCs were partially able to differentiate into SMA-positive tissues (Figure 4L). Quantitative analysis showed a greater percentage of GFP-positive cells and rat Y chromosome–positive cells, respectively, in the cell-sheet group compared with cell injection (Figure 4M). Quantitative analysis of vascular regeneration showed that the number of both GFP- and vWF-positive cells is 18±3/hpf (60% of GFP-positive cells), which participated in new blood vessel formation. In addition, the number of both Y chromosome– and SMA-positive cells is 7±2/hpf (45% of rat Y chromosome cells), which participated in new blood vessel formation. One week after treatment, a large number of integrin β1–positive cells were observed in the peri-infarct borderzone myocardium after cell-sheet therapy compared with cell injection and control (Figure 4N and 4O).

LV Remodeling After Cell-Sheet Transplantation

The LV myocardial structure was superiorly maintained after cell-sheet transplantation compared with cell injection and control, as assessed by hematoxylin-eosin staining (Figure 5A). In addition, cell-sheet therapy significantly attenuated collagen accumulation in the infarct area compared with cell injection and control, as demonstrated by Masson trichrome staining (Figure 5B and 5C).

Cardiac Functional Recovery After Cell-Sheet Transplantation

The effects of cocultured bi-level cell-sheet transplantation on cardiac function were assessed in a rat ICM model. After permanent occlusion of the LAD, EF, FS, and anterior wall thickness (baseline, 1.7±0.1 mm; at 2 weeks, 0.8±0.1 mm, at 4 weeks, 0.8±0.1 mm; P=0.0001, Kruskal–Wallis test) showed steady reductions, whereas EDD/ESD showed steady increases (EDD, P=0.0002; ESD, P=0.0001; Kruskal–Wallis test), suggesting progressive LV remodeling. After cocultured cell injection, the heart showed mild recovery, including increases in FS and EF. At 4 weeks after treatment, EF and FS tended to be greater after cocultured cell injection than the control; however, an even greater recovery was observed after cell-sheet transplantation (Figure 6A and 6B). At 4 weeks, the bi-level cell-sheet group had a significantly greater EF and FS and significantly improved EDD and ESD compared with either cell injection or control (Figure 6C and 6D).

Assessment by pressure–volume catheter further confirmed the cell-sheet–induced functional enhancement demonstrated by the echocardiographic data. Four weeks after transplantation, the maximal rate of change in LV pressure (max. dP/dt) and end-systolic pressure–volume relationship were significantly enhanced in the cell-sheet group compared with cell injection and control (Figure 7). Mimimal rate of change in LV pressure (min. dP/dt) and cardiac output were higher in the cell-sheet group than the other 2 groups, but the difference was not significant.

Discussion

This study revealed a multifaceted mechanism by which the targeted implantation of an EPC-SMC bi-level cell-sheet enhances myocardial function in a rodent model of ICM. A significant chemokine effect was observed in vitro where cocultured EPC-SMCs stimulated an abundant release of SDF1α, VEGF, HGF, and TGFβ; this effect is a mechanistic component of the augmented angiogenesis demonstrated in vivo. More importantly, however, the data clearly established direct migration of the cell-sheet EPCs and SMCs into the myocardium and confirmed these cells to be some elements of newly formed functional vasculature. The observed increased capillary density and improved blood perfusion in the borderzone elucidated the significant in vivo angiogenic potential of this technology. Furthermore, cell fate–tracking experiments strongly suggested the cell-sheet EPCs and SMCs as components of newly assembled vasculature. With regard to cell engraftment, the cell-sheet group performed superiorly, demonstrating improved cell–matrix attachment compared

Downloaded from http://circ.ahajournals.org/ at Osaka University on May 20, 2014

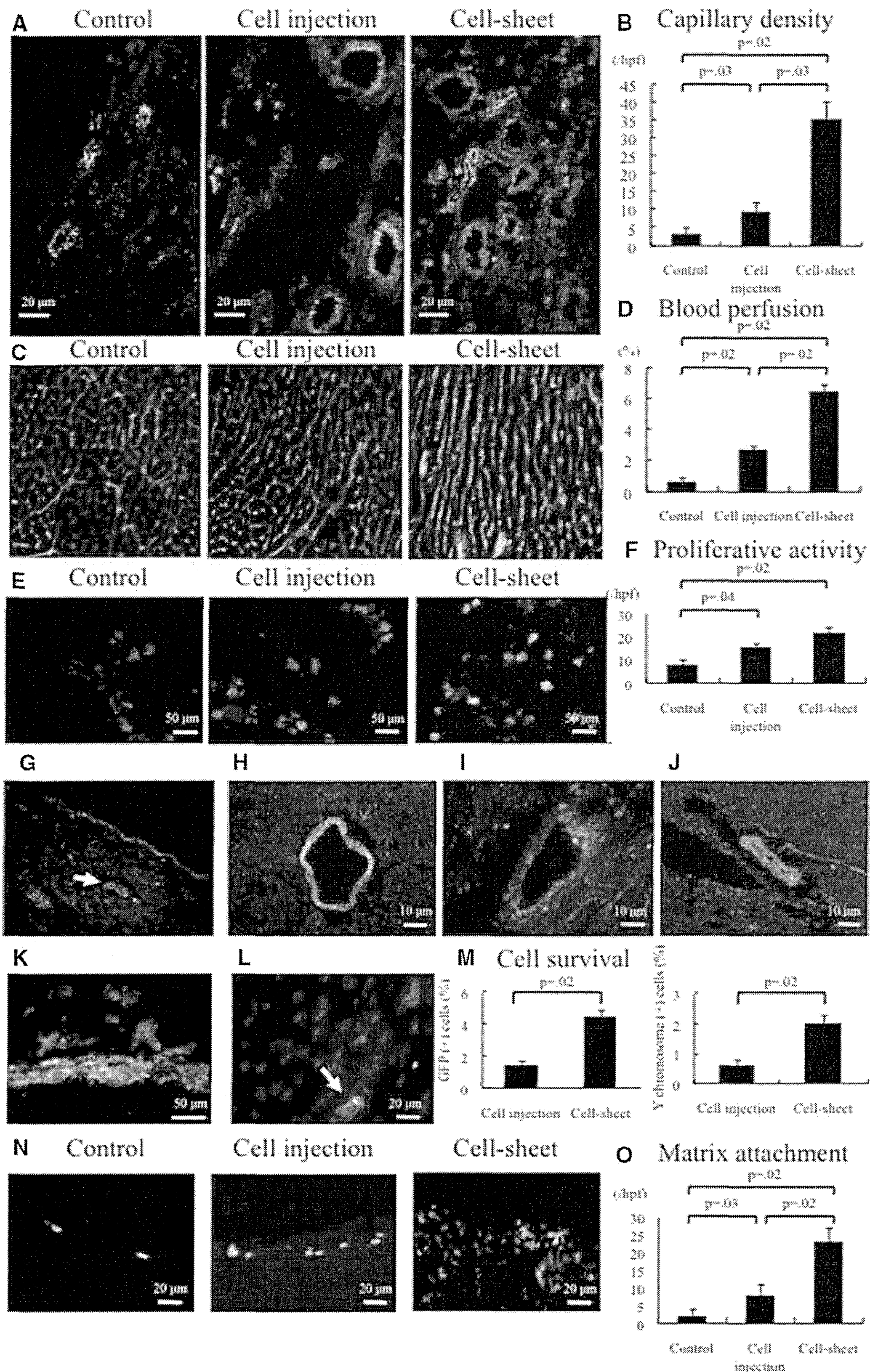

Figure 4. Effects on left ventricular remodeling, capillary density, and microvascular perfusion by bi-level cocultured cell-sheet transplantation (cell-sheet), cocultured cell injection (cell injection), and control (control) 4 weeks after the treatment procedure. **A**, Representative von Willebrand factor (vWF) staining of the borderzone myocardium. **B**, Quantification of capillary density. Capillary density was significantly enhanced in the cell-sheet groups compared with other groups (cell-sheet, n=4; cell injection, n=3; control, n=4; *P*=0.01, Kruskal–Wallis test). **C**, Representative lectin microangiographic imaging from the borderzone myocardium (×20 magnification). **D**, Quantitative analysis showed enhanced blood perfusion in the cell-sheet group compared with the other groups (cell sheet, n=4; cell injection, n=4; control, n=4; *P*=0.01, Kruskal–Wallis test). **E**, Representative antiproliferative cell nuclear

(*Continued*)

Downloaded from http://circ.ahajournals.org/ at Osaka University on May 20, 2014

Figure 4. Continued antigen staining of the borderzone myocardium. **F**, Quantification of cell proliferative activity. Proliferative activity was significantly enhanced in the cell-sheet group compared with control (cell sheet, n=4; cell injection, n=4; control, n=4; P=0.02, Kruskal–Wallis test). **G**, Immunoconfocal microscopy demonstrated abundant green fluorescent protein (GFP)-positive cells in the myocardium. **H**, Cryosections were stained with an antibody to vWF and GFP to detect the fate of endothelial progenitor cells (EPCs) in the heart. Immunostaining for vWF and GFP showed that transplanted EPCs over the borderzone myocardium were able to contribute directly to neovascularization of the host myocardium. Green indicates GFP; red, vWF; blue, nuclei. **I**, Immunostaining for vascular endothelial (VE)-cadherin and GFP showed that transplanted EPCs were able to contribute to neovascularization of the host myocardium. Green indicates GFP; red, VE-cadherin; blue, nuclei. **J**, In addition, staining with antibody to smooth muscle actin (SMA) and GFP demonstrated that GFP-positive EPCs originating from the transplanted cocultured bi-level cell sheet migrated into the treated myocardial tissues and were circumferentially supported by SMA-positive tissues. Green indicates GFP; red, SMA; blue, nuclei. **K**, Furthermore, to track SMCs from the cell sheet, we performed fluorescence in situ hybridization to identify male SMCs in the female recipient. Immediately after the cell-sheet transplantation, GFP-positive EPCs and Y chromosome–positive SMCs were detected in the epicardium. Red indicates rat Y chromosome; green, GFP. **L**, Rat Y chromosome SMCs were able to differentiate into SMA-positive tissues (white arrow). Red indicates SMA; yellow, rat Y chromosome; blue, nuclei. **M**, Quantitative analysis of cell survival estimation. GFP-positive cells and rat Y chromosome–positive cells were counted, respectively, and corrected by total number of tissue cells to examine the survival cells quantitatively. **N**, Representative anti-integrin β1 staining of the borderzone myocardium. **O**, Quantification of cell–matrix attachment. Cell–matrix attachment was significantly enhanced in the cell-sheet group compared with the other groups (cell sheet, n=4; cell injection, n=4; control, n=4; P=0.01, Kruskal–Wallis test).

with injection alone. The robust angiogenic effect of bi-level cell-sheet translated to enhanced myocardial function of the ischemic heart.

Our group has investigated the effects of EPCs as a neovasculogenic therapy for ICM using EPC therapy alone,[14] with seeded EPCs,[13] and with a tissue-engineered matrix.[2] Based on these findings, we began to explore the effects of ex vivo expanded EPCs. Systemic and direct myocardial injection of EPCs, however, is fraught with complications, such as cell dispersion and high percentages of cell loss. In this study, we used cell-sheet technology, which allows efficient delivery of cells onto the ischemic area of myocardium with minimal myocardial injury and cell dispersion, preserves cell–cell and cell–ECM architectural structure, and might, therefore, be more applicable to human translation.[15]

Given our previous work and experience with cell-sheet technology, one possible mechanism is likely to include cytokine release and hematopoietic stem cell recruitment.[7–9] Previous studies have shown that EPCs acted as the natural supplier of SDF1α,[16] VEGF,[17] HGF,[18] and TGFβ.[19] Their roles and signaling pathways have been intensively investigated; SDF1α is related to cell migration, proliferation, and migration[2,13,16]; VEGF is critical to stimulate endothelial cell proliferation and migration to initiate neovascularization[19]; HGF is beneficial to an impaired heart and is associated with an antifibrotic effect.[7,20] Together with our findings, it is reasonable to conclude that coculturing EPCs with SMCs enhanced the secretion of cytokines, such as SDF1α, VEGF, HGF, and TGFβ, compared with either EPCs or SMCs, thus leading to the enhanced proliferation of cardiomyocytes and stimulation of angiogenesis. To understand the detailed mechanism by which coculturing enhances cytokine secretion, we performed additional investigations from a new perspective. We found that FLK1 and VEGFR2 were upregulated by additional VEGF, which were even more enhanced by numerous cytokines containing cell-culturing medium, suggesting that multiple growth factors evoked the upregulation of FLK1 and VEGFR2 expressions over the single factor (ie, VEGF), thereby possibly amplifying VEGF release. The understanding of our results may be translated into the emerging concept that SMCs support the biological aspects of EPCs via the endothelial–pericyte cytokine cross-communication.

The mechanism of restoration of damaged myocardium by EPC transplantation is complex.[2,3,13] Although cytokine release and hematopoietic stem cell recruitment have been proposed as possible mechanisms of regeneration, other important mechanisms are likely to be involved. The creation of mature, stable, and functional vessels is essential. It has been reported

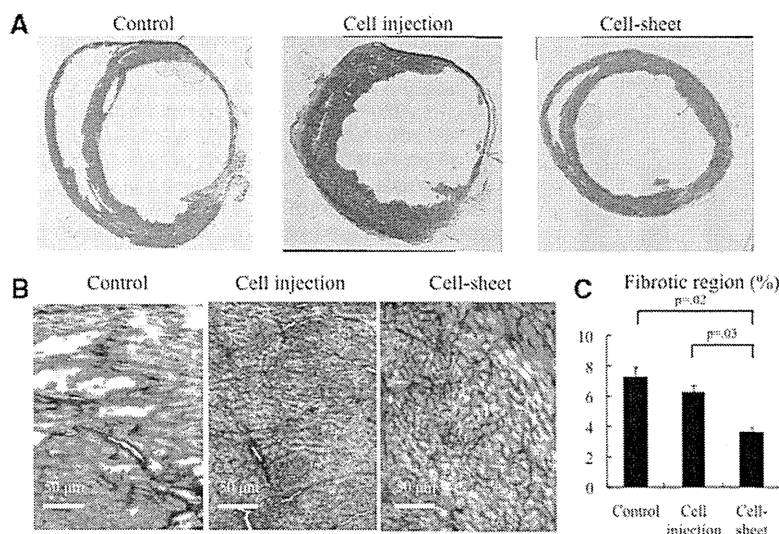

Figure 5. A, Representative macroscopic views of the heart (hematoxylin-eosin staining). The myocardial structure was superiorly maintained after cell-sheet transplantation compared with cell injection and control. **B**, Representative Masson trichrome staining at the borderzone myocardium. **C**, Quantification of fibrotic region. Fibrosis at the borderzone area was significantly suppressed in the cell-sheet group compared with the other groups (cell sheet, n=4; cell injection, n=3; control, n=4; P=0.02, Kruskal–Wallis test).

Downloaded from http://circ.ahajournals.org/ at Osaka University on May 20, 2014

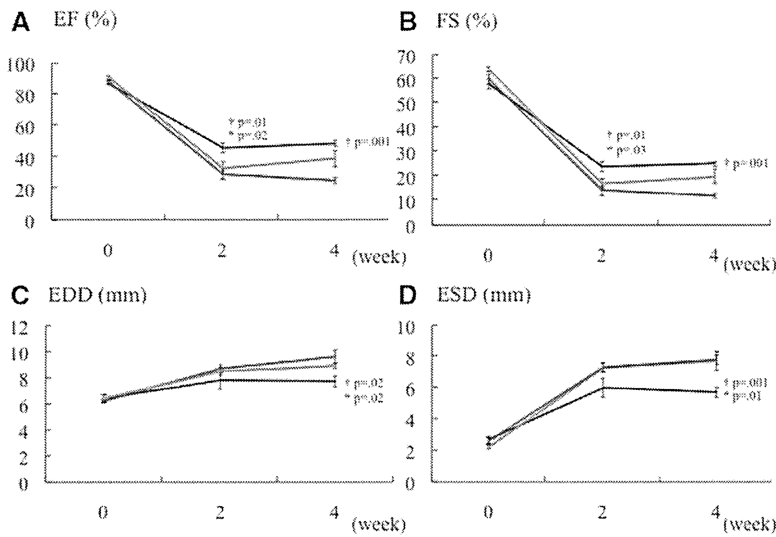

Figure 6. Serial changes in (**A**) ejection fraction (EF), (**B**) fractional shortening (FS), (**C**) end-diastolic diameter (EDD), and (**D**) end-systolic diameter (ESD) assessed by echocardiography (cell sheet, n=7, black line; cell injection, n=8, red line; control, n=9, blue line). Examinations were performed before (0) and at 2 and 4 weeks of follow-up after the operation. EF and FS were significantly higher at 2 and 4 weeks in the cell-sheet group compared with either cell injection or control (EF at 2 weeks, P=0.01; EF at 4 weeks, P=0.003; FS at 2 weeks, P=0.01; FS at 4 weeks, P=0.003; Kruskal–Wallis test). EDD and ESD were lowest at 4 weeks in the cell-sheet group (EDD, P=0.02; ESD, P=0.003; Kruskal–Wallis test). *P<0.05 vs cell injection; †P<0.05 vs control, post hoc pairwise Wilcoxon–Mann–Whitney U test.

that capillary formation occurs via two basic vessel-constructing processes: angiogenesis (ie, the formation of new capillaries via sprouting or intussusception from preexisting vessels) and vasculogenesis (ie, de novo formation of vasculature as occurs in the developing embryo).[21] It has also been reported that angiogenesis requires a dynamic temporally and spatially regulated interaction among endothelial cells, pericytes, and angiogenic factors.[22] Given the natural relationship between endothelium and intima within mature vessels, we added SMCs, which are essentially vascular pericytes, to enhance the angiogenic performance of EPCs. Thus, it was hypothesized that coculturing EPCs with SMCs would promote a robust angiogenic response and induce formation of mature blood vessels. Our present study shows that in addition to the

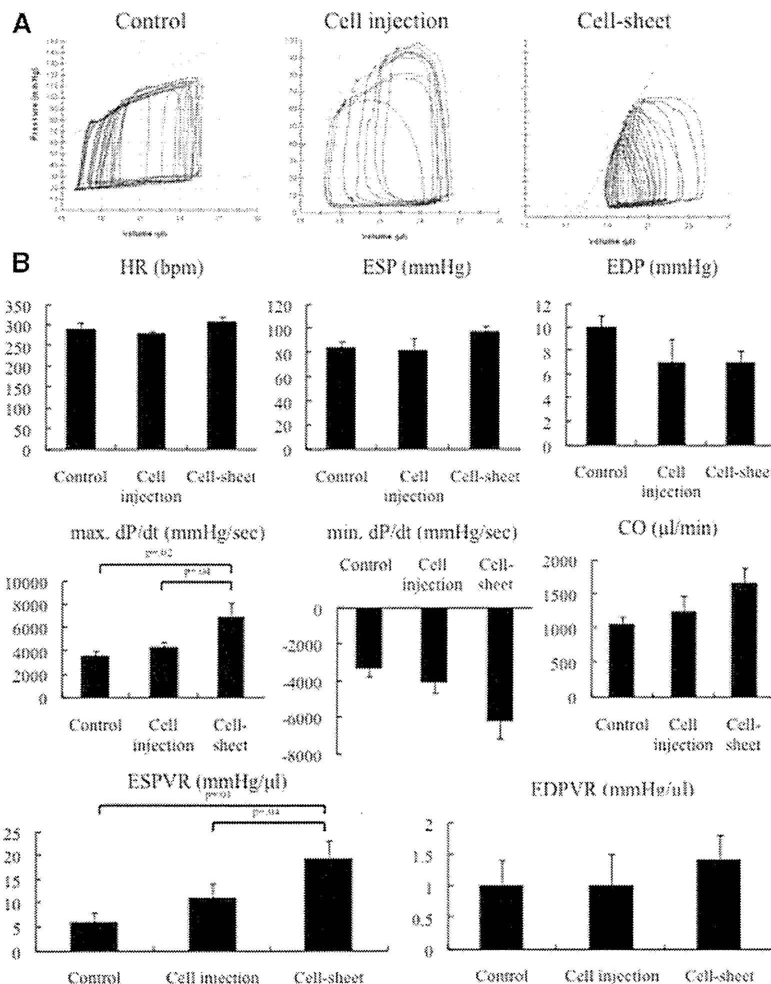

Figure 7. Hemodynamic measurements determined using cardiac catheterization after cocultured bi-level cell-sheet transplantation (cell-sheet, n=6), cocultured cell injection (cell injection, n=6), and control (control, n=8). Examinations were performed at 4 weeks of follow-up after the operation. **A**, Representative pressure–volume loops during inferior vena cava occlusion from cell-sheet, cell injection, and control groups. **B**, There was no significant difference in heart rate (HR), end-systolic pressure (ESP), end-diastolic pressure (EDP), mimimal rate of change in left ventricular (LV) pressure (min. dP/dt), cardiac output (CO), or end-diastolic pressure–volume relationship (EDPVR; HR, P=0.35; ESP, P=0.19; EDP, P=0.14; min. dP/dt, P=0.05; CO, P=0.07; EDPVR, P=0.70; Kruskal–Wallis test). The maximal rate of change in LV pressure (max. dP/dt) and end-systolic pressure–volume relationship (ESPVR) significantly improved in the cell-sheet group compared with the other 2 groups (max. dP/dt, P=0.04; ESPVR, P=0.03; Kruskal–Wallis test).

Downloaded from http://circ.ahajournals.org/ at Osaka University on May 20, 2014

increased capillary density and organized capillary network in the engineered myocardial tissues, enhanced GFP-labeled EPCs originating from the transplanted cell sheet seemed to differentiate into an inner vWF- and vascular endothelial-cadherin–positive endothelial layer surrounded by an outer circumferential SMA-positive layer, partially derived from transplanted SMCs. The direct contribution of SMCs was confirmed by fluorescence in situ hybridization analysis of the myocardium, demonstrating new vasculature containing male SMCs in a female heart. Furthermore, the morphology of the vessel formation within myocardial tissues, including the diameter, composition, and stability of vessel walls, suggested that vessel maturation may occur under pathological stimuli. Furthermore, our data showed that coculturing EPCs with SMCs enhanced the secretion of TGFβ, which is thought to promote stabilization in multiple ways: the synthesis and deposition of ECM and contextual regulation of proliferation and differentiation.[17] Therefore, it is likely that the process of vessel maturation is a transition from an actively growing vessel to a quiescent fully functional mature vessel network via endothelial–pericyte interaction.

The mechanism by which the transplanted cocultured bi-level cell sheet attenuated ventricular remodeling and improved cardiac function, as shown in this study, seemed to depend on the cell sheet being placed over the scarred area of the myocardium and led to repair of the anterior wall thickness, reduction of LV wall stress, and the improvement of LV function. Previous studies indicated that the surviving myocardium and transplanted cell sheet attenuate complex cellular and molecular events, including hypertrophy, fibrosis, apoptosis of the myocardium, and the pathological accumulation of ECM.[7,23]

Cell engraftment is another critical aspect of myocardial regeneration. The potential advantages of the cell-sheet technology include the ability to deliver a larger number of transplanted cells that integrate with native tissues without destroying the cell–cell or cell–ECM adhesions in the cell-sheet.[7] Together with our significant findings of increased cell survival, integrin β1 upregulation, and the enhanced secretion of HGF in vitro in the cell-sheet group, it is likely that the cocultured bi-level cell-sheet prolonged cell survival by preventing anoikis mediated by the ECM receptors, in particular via integrin β1, or modulated by growth factor (eg, HGF).[24]

This treatment strategy for acute myocardial infarction is not yet directly applicable to the clinical arena because of the time required to isolate, cultivate, and manipulate cells in vitro However, the finding that this therapy yielded marked cardioprotective effects through angiogenesis should be beneficial for treating other types of cardiac pathologies, such as the chronic phase of myocardial infarction.

A potential limitation of this study is that the optimal number of transplanted cells was unknown in vivo. In addition, further studies are necessary to determine the optimal mixing ratio of transplanted EPCs and SMCs. We believe that this scaffold-free cell-sheet technique seems to be more transplantable to humans.[15] Although the cocultured bi-level cell sheet maintained different cell types in separate layers in vitro, our in vivo findings showed that the transplanted cell sheet could be a mixture of both cell types. This is probably because each cell type possessed different cell affinity, cell–matrix attachment, and migration ability.

In conclusion, we found that coculturing EPCs with SMCs in a bi-level cell-sheet delivery system enhanced the angiogenic effect by facilitating more architecturally mature microvascular formation. We also observed that bi-level cell-sheet technology initiated robust angiogenesis and regulated vessel maturation, thereby reducing fibrosis, attenuating ventricular remodeling, and improving cardiac function in ischemic cardiomyopathic rats. These findings suggest that novel bi-level cell-sheet technology creates an avenue of powerful cardiac repair. This concept may lead to new regeneration therapies in advanced cardiomyopathy.

Acknowledgments

We thank Dr Arudo Hiraoka, Dr Masaki Taira, and Akima Harada for their excellent technical assistances. We also thank Dr Takashi Daimon, Department of Biostatistics, Hyogo College of Medicine, for his statistical assessment.

Sources of Funding

This study was supported by the National Institutes of Health grant 1R01HL089315 (to Dr Woo), the American Heart Association Great Rivers Affiliate Postdoctoral Fellowship cosponsored by the Claude R. Joyner Fund for Young Medical Researchers (No. 12POST12060567; to Dr Shudo), and the Shinya Fund for International Exchange, Japan (Dr Shudo).

Disclosures

None.

References

1. Hiesinger W, Perez-Aguilar JM, Atluri P, Marotta NA, Frederick JR, Fitzpatrick JR 3rd, McCormick RC, Muenzer JR, Yang EC, Levit RD, Yuan LJ, Macarthur JW, Saven JG, Woo YJ. Computational protein design to reengineer stromal cell-derived factor-1α generates an effective and translatable angiogenic polypeptide analog. *Circulation.* 2011;124(11 suppl):S18–S26.
2. Frederick JR, Fitzpatrick JR 3rd, McCormick RC, Harris DA, Kim AY, Muenzer JR, Marotta N, Smith MJ, Cohen JE, Hiesinger W, Atluri P, Woo YJ. Stromal cell-derived factor-1alpha activation of tissue-engineered endothelial progenitor cell matrix enhances ventricular function after myocardial infarction by inducing neovasculogenesis. *Circulation.* 2010;122(11 suppl):S107–S117.
3. Atluri P, Panlilio CM, Liao GP, Hiesinger W, Harris DA, McCormick RC, Cohen JE, Jin T, Feng W, Levit RD, Dong N, Woo YJ. Acute myocardial rescue with endogenous endothelial progenitor cell therapy. *Heart Lung Circ.* 2010;19:644–654.
4. Hagège AA, Marolleau JP, Vilquin JT, Alhéritière A, Peyrard S, Duboc D, Abergel E, Messas E, Mousseaux E, Schwartz K, Desnos M, Menasché P. Skeletal myoblast transplantation in ischemic heart failure: long-term follow-up of the first phase I cohort of patients. *Circulation.* 2006;114(1 suppl):I108–I113.
5. Schächinger V, Erbs S, Elsässer A, Haberbosch W, Hambrecht R, Hölschermann H, Yu J, Corti R, Mathey DG, Hamm CW, Süselbeck T, Assmus B, Tonn T, Dimmeler S, Zeiher AM; REPAIR-AMI Investigators. Intracoronary bone marrow-derived progenitor cells in acute myocardial infarction. *N Engl J Med.* 2006;355:1210–1221.
6. Assmus B, Honold J, Schächinger V, Britten MB, Fischer-Rasokat U, Lehmann R, Teupe C, Pistorius K, Martin H, Abolmaali ND, Tonn T, Dimmeler S, Zeiher AM. Transcoronary transplantation of progenitor cells after myocardial infarction. *N Engl J Med.* 2006;355:1222–1232.
7. Miyagawa S, Roth M, Saito A, Sawa Y, Kostin S. Tissue-engineered cardiac constructs for cardiac repair. *Ann Thorac Surg.* 2011;91:320–329.
8. Imanishi Y, Miyagawa S, Maeda N, Fukushima S, Kitagawa-Sakakida S, Daimon T, Hirata A, Shimizu T, Okano T, Shimomura I, Sawa Y. Induced adipocyte cell-sheet ameliorates cardiac dysfunction in a mouse

Downloaded from http://circ.ahajournals.org/ at Osaka University on May 20, 2014

myocardial infarction model: a novel drug delivery system for heart failure. *Circulation*. 2011;124(11 suppl):S10–S17.

9. Shudo Y, Miyagawa S, Fukushima S, Saito A, Shimizu T, Okano T, Sawa Y. Novel regenerative therapy using cell-sheet covered with omentum flap delivers a huge number of cells in a porcine myocardial infarction model. *J Thorac Cardiovasc Surg*. 2011;142:1188–1196.
10. Sekine H, Shimizu T, Hobo K, Sekiya S, Yang J, Yamato M, Kurosawa H, Kobayashi E, Okano T. Endothelial cell coculture within tissue-engineered cardiomyocyte sheets enhances neovascularization and improves cardiac function of ischemic hearts. *Circulation*. 2008;118(14 suppl):S145–S152.
11. Kobayashi H, Shimizu T, Yamato M, Tono K, Masuda H, Asahara T, Kasanuki H, Okano T. Fibroblast sheets co-cultured with endothelial progenitor cells improve cardiac function of infarcted hearts. *J Artif Organs*. 2008;11:141–147.
12. Dzau VJ, Braun-Dullaeus RC, Sedding DG. Vascular proliferation and atherosclerosis: new perspectives and therapeutic strategies. *Nat Med*. 2002;8:1249–1256.
13. Atluri P, Liao GP, Panlilio CM, Hsu VM, Leskowitz MJ, Morine KJ, Cohen JE, Berry MF, Suarez EE, Murphy DA, Lee WM, Gardner TJ, Sweeney HL, Woo YJ. Neovasculogenic therapy to augment perfusion and preserve viability in ischemic cardiomyopathy. *Ann Thorac Surg*. 2006;81:1728–1736.
14. Asahara T, Murohara T, Sullivan A, Silver M, van der Zee R, Li T, Witzenbichler B, Schatteman G, Isner JM. Isolation of putative progenitor endothelial cells for angiogenesis. *Science*. 1997;275:964–967.
15. Sawa Y, Miyagawa S, Sakaguchi T, Fujita T, Matsuyama A, Saito A, Shimizu T, Okano T. Tissue engineered myoblast sheets improved cardiac function sufficiently to discontinue LVAS in a patient with DCM: report of a case. *Surg Today*. 2012;42:181–184.
16. Urbich C, Aicher A, Heeschen C, Dernbach E, Hofmann WK, Zeiher AM, Dimmeler S. Soluble factors released by endothelial progenitor cells promote migration of endothelial cells and cardiac resident progenitor cells. *J Mol Cell Cardiol*. 2005;39:733–742.
17. Li M, Nishimura H, Iwakura A, Wecker A, Eaton E, Asahara T, Losordo DW. Endothelial progenitor cells are rapidly recruited to myocardium and mediate protective effect of ischemic preconditioning via “imported” nitric oxide synthase activity. *Circulation*. 2005;111:1114–1120.
18. Rehman J, Li J, Orschell CM, March KL. Peripheral blood “endothelial progenitor cells” are derived from monocyte/macrophages and secrete angiogenic growth factors. *Circulation*. 2003;107:1164–1169.
19. Coussens LM, Werb Z. Inflammation and cancer. *Nature*. 2002;420:860–867.
20. Madonna R, Rokosh G, De Caterina R, Bolli R. Hepatocyte growth factor/Met gene transfer in cardiac stem cells–potential for cardiac repair. *Basic Res Cardiol*. 2010;105:443–452.
21. Risau W. Mechanisms of angiogenesis. *Nature*. 1997;386:671–674.
22. Goumans MJ, Valdimarsdottir G, Itoh S, Rosendahl A, Sideras P, ten Dijke P. Balancing the activation state of the endothelium via two distinct TGF-beta type I receptors. *EMBO J*. 2002;21:1743–1753.
23. Golocheikine A, Tiriveedhi V, Angaswamy N, Benshoff N, Sabarinathan R, Mohanakumar T. Cooperative signaling for angiogenesis and neovascularization by VEGF and HGF following islet transplantation. *Transplantation*. 2010;90:725–731.
24. Zvibel I, Smets F, Soriano H. Anoikis: roadblock to cell transplantation? *Cell Transplant*. 2002;11:621–630.

Downloaded from http://circ.ahajournals.org/ at Osaka University on May 20, 2014

EUROPEAN SOCIETY OF CARDIOLOGY®

Cardiovascular Research (2013) **99**, 102–110
doi:10.1093/cvr/cvt088

Transplantation of myoblast sheets that secrete the novel peptide SVVYGLR improves cardiac function in failing hearts

Ayako Uchinaka[1], Naomasa Kawaguchi[1,2*], Yoshinosuke Hamada[1], Seiji Mori[1], Shigeru Miyagawa[3], Atsuhiro Saito[4], Yoshiki Sawa[3], and Nariaki Matsuura[1]

[1]Department of Molecular Pathology, Osaka University Graduate School of Medicine, Suita, Japan; [2]Department of Cardiovascular Pathology, Division of Health Sciences, Osaka University Graduate School of Medicine, Suita, Japan; [3]Department of Cardiovascular Surgery, Osaka University Graduate School of Medicine, Suita, Japan; and [4]Medical Center of Translational Research, Osaka University Hospital, Osaka University Graduate School of Medicine, Suita, Japan

Received 4 December 2012; revised 27 March 2013; accepted 7 April 2013; online publish-ahead-of-print 23 April 2013

Time for primary review: 52 days

Aims Transplantation of myoblast sheets is a promising therapy for enhancing cardiac function after heart failure. We have previously demonstrated that a 7-amino-acid sequence (Ser-Val-Val-Tyr-Gly-Leu-Arg) derived from osteopontin (SV peptide) induces angiogenesis. In this study, we evaluated the long-term therapeutic effects of myoblast sheets secreting SV in a rat infarction model.

Methods and results Two weeks after ligation of the left anterior descending coronary artery, the animals were divided into the following three groups: a group transplanted with wild-type rat skeletal myoblast sheets (WT-rSkMs); a group transplanted with SV-secreting myoblast sheets (SV-rSkMs); and a control group (ligation only). We evaluated cardiac function, histological changes, and smooth muscle actin (SMA) expression through transforming growth factor-β (TGF-β) signalling. The ejection fraction and fractional shortening were significantly better, and the enlargement of end-systolic volume was also significantly attenuated in the SV-rSkM group. Left ventricular remodelling, including fibrosis and hypertrophy, was significantly attenuated in the SV-rSkM group, and SV secreted by the myoblast sheets promoted angiogenesis in the infarcted border area. Furthermore, many clusters of SMA-positive cells were observed in the infarcted areas in the SV-rSkM group. *In vitro* SMA expression was increased when SV was added to the isolated myocardial fibroblasts. Moreover, SV bound to the TGF-β receptor, and SV treatment activated TGF-β receptor–Smad signalling.

Conclusion The SV-secreting myoblast sheets facilitate a long-term improvement in cardiac function. The SV can induce differentiation of fibroblasts to myofibroblasts via TGF-β–Smad signalling. This peptide could possibly be used as a bridge to heart transplantation or as an ideal peptide drug for cardiac regeneration therapy.

Keywords Cell therapy • Peptides • Myocardial infarction • Myofibroblats • Transforming growth factor-β

1. Introduction

In heart failure, tissue damage processes caused by ischaemia, such as cell death, fibrosis, and hypertrophy, gradually progress until the cardiac tissue becomes dysfunctional.[1–3] Transplantation of myoblast sheets is a promising treatment for ischaemic heart failure, and can inhibit left ventricular (LV) remodelling and improve cardiac function via paracrine effectors.[4–8] The cell-sheet technique avoids the arrhythmogenicity associated with skeletal myoblast therapy by injection.[9]

However, this treatment has failed to achieve long-term therapeutic effects, because the transplanted sheets are exposed to blood and nutrient deprivation and drop out from the injured myocardium. Recent studies demonstrated that myoblast sheets that overexpress different cardioprotective agents display enhanced therapeutic effects.[10,11] Therefore, the combined application of gene therapy with angiogenic agents and myoblast sheet transplantation may achieve sustained therapeutic efficacy. Through the secretion of angiogenic factors from transplanted myoblasts, the newly formed blood vessels can supply blood flow to the surviving myocardium and the transplanted

* Corresponding author: 1-7 Yamada-oka, Suita, Osaka 565-0871, Japan. Tel: +81 6 6879 2588; fax: +81 6 6879 2588, E-mail: kawaguch@sahs.med.osaka-u.ac.jp

Published on behalf of the European Society of Cardiology. All rights reserved. © The Author 2013. For permissions please email: journals.permissions@oup.com.

Downloaded from http://cardiovascres.oxfordjournals.org/ at Osaka University on May 20, 2014

cells, and the functional deterioration of ischaemic cardiomyopathy should thus improve in the long term.

Osteopontin is a multifunctional cytokine expressed during healing and fibrotic processes.[12] We have previously reported that the osteopontin-derived peptide Ser-Val-Val-Tyr-Gly-Leu-Arg (SVVYGLR; SV) exhibits angiogenic activity *in vitro* and *in vivo*,[13–17] and that its angiogenic activity is as potent as that of vascular endothelial growth factor (VEGF).[14] Owing to their high molecular weights, the most well-known angiogenesis-promoting factors, namely, VEGF and hepatocyte growth factor (HGF), are resistant to degradation. In contrast, peptides such as SV are more easily degraded by peptidase within an organism and show only a few adverse effects, such as oedema and pleural fluid accumulation.[18–20] This indicates the high biocompatibility of peptides.

In this study, we hypothesized that the augmentation of myoblast sheets by SV gene transfer could improve cardiac function in the long term.

2. Methods

2.1 Animal ethics

Animal care complied with the 'Guide for Care and Use of Laboratory Animals' (NIH publication no. 85-23, revised 1996). The Ethics Review Committee for Animal Experimentation of Osaka University Graduate School of Medicine approved the experimental protocols.

2.2 Isolation of skeletal myoblasts and sheets

After induction of general anaesthesia with pentobarbital (300 mg/kg) and heparin (150 U) by intraperitoneal injection, myoblasts were isolated from the skeletal muscle of the tibialis anterior muscle of 3-week-old male Lewis rats. The muscles were minced and enzymatically dissociated with 0.2% collagenase type II (Worthington Biochemical Corp., Lakewood, NJ, USA) and trypsin at 37°C. The isolated cells were suspended in Dulbecco's modified Eagle's medium with 20% fetal bovine serum. After being preplated twice, non-adherent cells were then plated on a dish coated with Matrigel (Becton Dickinson Bioscience, Franklin Lakes, NJ, USA) and incubated at 37°C in humidified air enriched with 5% CO_2. We maintained the cell densities at $<$70% confluence to prevent skeletal myoblast differentiation that would result in myotube formation. Myoblast sheets were formed by plating 3×10^6 infected myoblasts on a temperature-responsive culture dish (UpCell; CellSeed, Tokyo, Japan).

2.3 Animal model and myoblast sheet transplantation

The myocardial infarction (MI) models were generated via ligation of the left anterior descending (LAD) coronary artery in 8-week-old female F344/NJcl-rnu/rnu rats. The rats were anaesthetized by inhalation of isoflurane (2%, 0.2 mL/min), intubated, and placed on a respirator during surgery to maintain ventilation. The carrier gas for isoflurane is oxygen. The adequacy of anaesthesia was monitored by electrocardiography and pulse rate. Two weeks after ligation of the LAD coronary artery, the myoblast sheets were transplanted. The rats were randomly divided into the following three groups: (i) a WT-rat skeletal myoblast (rSkM) group (transplanted with three wild-type myoblast sheets, $n = 6$); (ii) an SV-rSkM group (transplanted with three SV-secreting myoblast sheets, $n = 8$); and (iii) a control group (sham operation, $n = 6$). Each sheet was individually applied to the infarcted area.

2.4 Overexpression and transfection of SV

A lentiviral vector containing the complementary DNA (cDNA) of SV (SV/pCS-CG) was constructed (*Figure 1A*). The cDNA of SV was synthesized using DNA oligonucleotides. The primer sequences were as follows: forward, 1,5′-GCGCCACCATGGAGACAGACACACTCCTGCTATGG GTACTGCTGCTCTGGGTTCCAGGT-3′; forward, 2,5′-TCCACTGGT GACGCGGCCCAGCCGGCCAGTGTGGTTTATGGACTGAGGCTC GAGTACCCATACGATGTTCCAGATTACGCTTAAC-3′; reverse, 1,5′-TCGAGTTAAGCGTAATCTGGAACATCGTATGGGTACTCGA GCCTCAGTCCATAAACCACACT-3′; and reverse, 2,5′-GGCCGGC TGGGCCGCGTCACCAGTGGAACCTGGAACCCAGAGCAGCAGTA CCCATAGCAGGAGTGTGTCTGTCTCCATGGTGGCG-3′.

The synthesized DNA oligonucleotides were linked and ligated to pCS-CG, and the isolated rSkMs were infected via incubation for 48 h in the presence of SV/pCS-CG.

2.5 Dot blotting assay

The culture media were used for the assays. Each sample was coated onto a black 96-well microplate overnight. To evaluate the secretion SV volume, the serially diluted solution of SV-HA peptide was also coated onto the plate as a control. After blocking, the primary antibody against the HA tag (Santa Cruz Biotechnology, Santa Cruz, CA, USA) was added to each well. After washing, anti-rabbit IgG-linked horseradish peroxidase (GE Healthcare, Piscataway, NJ, USA) was added. After washing, the plate was exposed to an Enhanced Chemiluminescence (ECL) kit (GE Healthcare).

2.6 Measurement of cardiac function

The cardiac function of the treated rats was evaluated by echocardiography 2, 4, 6, and 8 weeks after sheet transplantation. Baseline measurements were

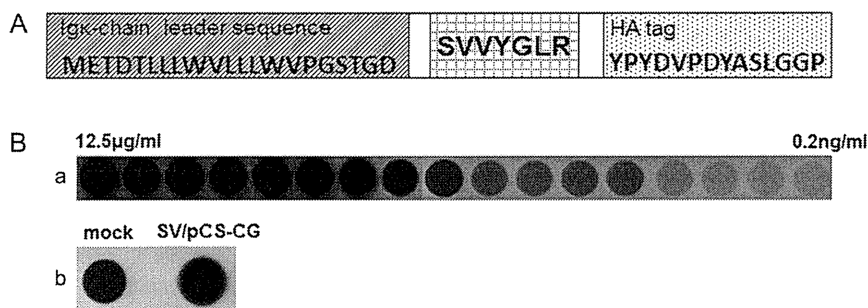

Figure 1 Assessment of SV expression. (*A*) View showing the frame format of the constructed SV gene. (*B*) Expression of SV in rSkMs infected with SV/pCS-CG by dot blotting: (*a*) the dilution series of SV-HA peptide; and (*b*) control cells infected with the empty vector (mock, left) and rSkMs infected with SV/pCS-CG (right).

made before sheet transplantation. The measurements were made using a SONOS 5500 sonograph (Philips Electronics, Tokyo, Japan) with a 12 MHz transducer under general anaesthesia induced and maintained by inhalation of isoflurane (2%, 0.2 mL/min) as mentioned above. The LV end-systolic area, LV end-diastolic area, and LV dimensions at end diastole and end systole (LVIDd and LVIDs, respectively) were determined. The ejection fraction (EF), fractional shortening (FS), end-diastolic volume (EDV), and end-systolic volume (ESV) were calculated as follows:

$$LVEF (\%) = (LVDd^3 - LVDs^3)/LVDd^3 \times 100 (\%)$$
$$LV\%FS = [(LVDd - LVDs)/LVDd] \times 100 (\%)$$
$$EDV = LVIDd^3 \times (0.98 \times LVIDd + 5.90) (mL)$$
$$ESV = LVIDs^3 \times (1.14 \times LVIDs + 4.18) (mL)$$

2.7 Heart weight/body weight ratio

The body weights (BW; in grams) of the rats were measured 8 weeks after sheet transplantation, after which the rats were anaesthetized with pentobarbital (300 mg/kg) and heparin (150 U) by intraperitoneal injection, and their hearts were rapidly removed and weighed (in milligrams). The heart weight (HW)/BW ratio was then calculated.

2.8 Histological analyses

Myocardial specimens were obtained 8 weeks post-transplantation. The formalin-fixed samples were embedded in paraffin. The LV chamber diameter and the anterior wall thickness were measured from sections stained with haematoxylin and eosin. Infarcted wall thickness, posterior wall thickness, and LV chamber diameter were measured with the scale loupe. The sections were evaluated morphologically using the NIS Elements system (Nikon, Tokyo, Japan). Sirius Red staining was used to detect fibrosis. The percentage of fibrosis was calculated from the fibrotic ratio in the infarct border area. Periodic acid–Schiff staining for cardiomyocyte hypertrophy was also performed. We randomly selected 100 cardiomyocytes and measured the two-point shortest axes at the level of the nucleus.

Immunohistochemical staining for von Willebrand factor antigen was used to label vascular endothelial cells to permit the counting of blood vessels. The sections were incubated with primary antibody against von Willebrand factor (rabbit polyclonal; Dako, Glostrup, Denmark). The sections were incubated with a biotinylated anti-rabbit IgG antibody (Dako) and further incubated with peroxidase-conjugated streptavidin (SA; GE Healthcare). Visualization was performed with biphenyl-3,3′,4,4′-tetramine solution (Sigma, St Louis, MO, USA). The stained vascular endothelial cells were counted under a light microscope.

The distribution of myofibroblast-like cells was evaluated by immunohistochemical staining with anti-smooth muscle actin (SMA) antibody (Dako) and anti-smooth muscle myosin heavy chain (SM-MHC) type 2 antibody (Abcam Ltd, Cambridge, UK). The SMA-positive cell density was calculated as SMA positive area/infarcted area × 100 (%).

2.9 Primary culture of adult ventricular fibroblasts

Cardiac fibroblasts (CFs) were isolated from 8-week-old adult male Sprague–Dawley rats 4 weeks after the induction of MI by LAD ligation. The hearts were excised from anaesthetized rats and quickly transferred to Hank's buffered salt solution. The minced left ventricular tissues were digested using 100 U/mL type II collagenase and 0.1% trypsin at 37°C. The cells were centrifuged and suspended in Dulbecco's modified Eagle's medium supplemented with 10% fetal bovine serum, and incubated at 37°C in humidified air enriched with 5% CO_2.

2.10 Immunofluorescence staining

The isolated fibroblasts were incubated with SV (10 μg/mL), SV random peptide (GYRVLSV; 10 μg/mL), or transforming growth factor-β1 (TGF-β1; 25 ng/mL) for 72 h. The cells were fixed with 4% paraformaldehyde and incubated with anti-SMA antibody followed by incubation with cyanine-3-conjugated anti-rabbit secondary antibody (GE Healthcare). The nuclei were stained with 4′,6-diamino-2-phenylindole (DAPI; Invitrogen Life Technologies, Grand Island, NY, USA), and the fluorescent signals were detected by fluorescence microscopy (ECLIPSE E600, Nikon).

2.11 Western blotting assay

The isolated fibroblasts were incubated with SV (10 μg/mL), SV random peptide (10 μg/mL), or TGF-β1 (25 ng/mL) for 72 h. The cells were suspended in lysis buffer (50 mM Tris at pH 8.0, 120 mM NaCl, 1 mM EDTA, and 0.5% Nonidet P-40). Proteins in whole-cell lysates were separated by SDS–PAGE, transferred to a polyvinylidene fluoride transfer membrane (Millipore, Billerica, MA, USA), and probed sequentially with antibodies against SMA and α-tubulin (Sigma). The blots were developed using an ECL kit.

To examine the activity of TGF-β receptor–Smad signalling induced by SV, the phosphorylation of Smad2, Smad3, and TGF-β receptor I (TβRI) was studied by western blotting. The isolated fibroblasts were incubated with SV (10 μg/mL), SV random peptide (10 μg/mL), or TGF-β1 (25 ng/mL) for 1 h. Primary antibodies against phospho-Smad2, phospho-Smad3, Smad2/3 (Cell Signaling Technology, Inc., Danvers, MA, USA), TβRI (phospho S165; Abcam), and α-tubulin were used.

2.12 Construction of recombinant transforming growth factor-β receptorII

A pcDNA3.1 vector containing the cDNA encoding TβRII (pcDNA3.1-TβRII) was constructed. The recombinant TβRII was produced by transfecting HEK 293T cells with pcDNA3.1-TβRII. The culture media containing recombinant TβRII were harvested. The purification of recombinant TβRII was done using immunoprecipitation with anti-TβRII antibody.

2.13 Biacore analysis

The binding of SV to TβRII was assessed by Biacore analysis. Biotinylated SVs were captured on SA-coated BIAcore SA sensor chips (GE Healthcare, Piscataway, NJ, USA). Ligands were diluted to 10 μg/mL and injected at 10 μL/mL. To correct for refractive index change, non-specific binding, and instrument drift, a reference flow cell contained the SA-coated surface only. The recombinant TβRII was diluted to 10 μg/mL in Hank's buffered salt solution and injected during the association phase for 5 min (30 μL/min).

2.14 *In situ* proximity ligation assay

The Duolink *in situ* proximity ligation assay (PLA; Olink Biosciences, Uppsala, Sweden) was performed according to the manufacturer's protocol. The isolated fibroblasts were incubated in the presence of SV-HA peptide or SV-HA random peptide (GYRVLSV; 1 μg/mL) for 1 h. The fixed fibroblasts were incubated with the following primary antibodies: rabbit polyclonal anti-TβRII (Abcam) and mouse monoclonal anti-HA (Nacalai Tesque). The cells were then incubated with PLA probes consisting of two secondary anti-rabbit and anti-mouse antibodies, each tagged with an oligonucleotide. A hybridization solution consisting of two oligonucleotide linkers complementary to each PLA probe was added to the cells. The isolated cells were incubated with a Duolink Ligation stock containing ligase and Duolink polymerase. In addition, the cells were incubated with a detection solution consisting of fluorescently labelled oligonucleotides that hybridize to the rolling circle amplification product. The PLA signal was visualized using fluorescence microscopy.

2.15 Statistical analyses

Data are presented as the means ± SEM. Cardiac function was analysed by repeated-measures analysis of variance (ANOVA) for differences across the entire time course, as well as one-way ANOVA, whereas the Tukey–Kramer *post hoc* test was used to examine significant differences at each time point. To assess the significance of the differences between individual groups for

Downloaded from http://cardiovascres.oxfordjournals.org/ at Osaka University on May 20, 2014

other data, statistical comparisons were performed using Student's unpaired *t*-test. $P < 0.05$ was considered statistically significant.

3. Results

3.1 Overexpression of SV in rat skeletal myoblasts

The signal strength of dots in wells coated with the culture medium of SV/pCS-CG-infected rSkMs was stronger than that of dots in wells coated with the culture medium of mock-infected rSkMs (*Figure 1B*[*b*]). The SV was synthesized and secreted by SV/pCS-CG-infected rSkMs. In addition, from the dilution series of SV-HA peptide, the secretion volume of SV was calculated to be approximately 3.125–6.25 ng/mL (*Figure 1B*[*a*]).

3.2 Effect of SV-secreting myoblast sheet on left ventricular function

Echocardiography revealed significantly better values of LVEF and %FS in the WT-rSkM and SV-rSkM groups compared with the control group at all time points after transplantation ($P < 0.01$). Although there were still significant differences between the control and WT-rSkM groups after the 4 week time point, the LVEF and %FS in the WT-rSkM group decreased dramatically. Furthermore, LVEF and %FS were significantly better in the SV-rSkM group at 2, 6, and 8 weeks after transplantation compared with the WT-rSkM group (2 and 6 weeks, $P < 0.05$; 8 weeks, $P < 0.01$; *Figure 2A* and *B*).

The evaluation of LVIDs illustrated the inhibition of dilatation in the SV-rSkM group in comparison with the control and WT-rSkM groups. In particular, at 6 and 8 weeks after transplantation LVIDs was significantly attenuated in the SV-rSkM group compared with the control group (6 weeks $P < 0.05$; 8 weeks $P < 0.01$; *Table 1*). The enlargement of ESV was also significantly attenuated in the SV-rSkM group compared with the control group at 6 and 8 weeks after transplantation (6 weeks, $P < 0.05$; 8 weeks, $P < 0.01$; *Table 1*). The increase in EDV was significantly inhibited in the SV-rSkM group compared with the control group only at 8 weeks after transplantation ($P < 0.05$; *Table 1*).

3.3 Heart weight/body weight ratio

We used the HW/BW ratio as an indicator of cardiac hypertrophy. The HW/BW ratio was significantly greater in the SV-rSkM group at 8 weeks after transplantation compared with the control and WT-rSkM groups ($P < 0.01$; *Figure 2C*).

3.4 Effect of SV-secreting myoblast sheet on left ventricular remodelling

Haematoxylin and eosin staining demonstrated thinning of the infarcted wall in the control and WT-rSkM groups, whereas the thickness of the infarcted wall was maintained in the SV-rSkM group (*Figure 2D* and *Table 2*). Statistical analysis demonstrated that the LV chamber of the SV-rSkM group was significantly less dilated that those of the control and WT-rSkM groups ($P < 0.05$; *Table 2*) and that the infarcted wall in the SV-rSkM group was significantly thicker than that in the control

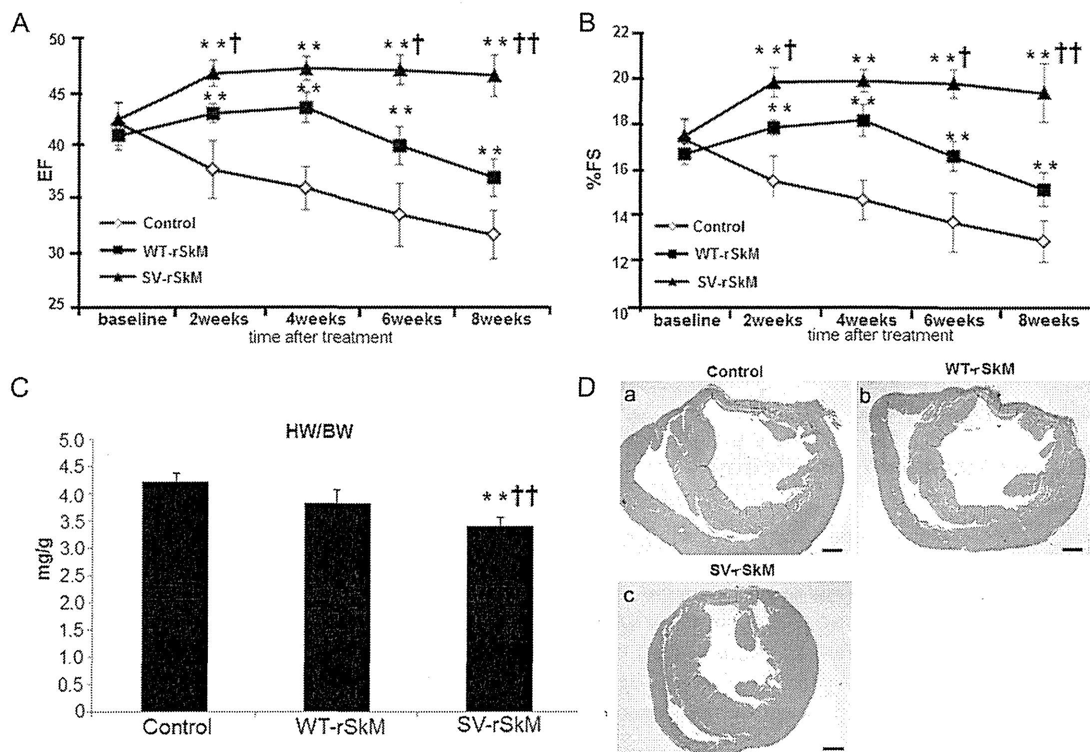

Figure 2 Echocardiographic evaluation of LV function after sheet transplantation (*A*, EF; *B*, %FS). $^{**}P < 0.01$ vs. Control group. $^{\dagger}P < 0.05$, $^{\dagger\dagger}P < 0.01$ vs. WT-rSkM group. Baseline is time of transplantation, which was 2 weeks after ligation of the LAD. Other times in weeks are post-transplantation. (*C*) Evaluation of HW/BW. $^{**}P < 0.01$ vs. Control group. $^{\dagger}P < 0.05$, $^{\dagger\dagger}P < 0.01$ vs. WT-rSkM group. (*D*) Haematoxylin- and eosin-stained section of the left ventricle: (*a*) control; (*b*) WT-rSkM; and (*c*) SV-rSkM (×10 magnification, scale bars represent 1000 μm).

Table 1 Assessment of LVIDd, LVIDs, EDV, and ESV over time by echocardiography

	Baseline	2 weeks	4 weeks	6 weeks	8 weeks
LVIDd (cm)					
Control	0.75 ± 0.04	0.77 ± 0.07	0.81 ± 0.05	0.87 ± 0.04	0.89 ± 0.01
WT-rSkM	0.76 ± 0.02	0.77 ± 0.04	0.80 ± 0.06	0.84 ± 0.06	0.85 ± 0.03
SV-rSkM	0.71 ± 0.05	0.78 ± 0.07	0.78 ± 0.07	0.83 ± 0.03	0.84 ± 0.03*
LVIDs (cm)					
Control	0.63 ± 0.02	0.67 ± 0.05	0.70 ± 0.05	0.75 ± 0.04	0.77 ± 0.02
WT-rSkM	0.63 ± 0.02	0.64 ± 0.03	0.67 ± 0.06	0.69 ± 0.05	0.72 ± 0.04
SV-rSkM	0.64 ± 0.04	0.65 ± 0.05	0.67 ± 0.04	0.67 ± 0.03*	0.69 ± 0.04**
EDV (ml)					
Control	2.87 ± 0.46	3.19 ± 0.93	3.65 ± 0.71	4.46 ± 0.63	4.79 ± 0.26
WT-rSkM	2.93 ± 0.24	3.04 ± 0.43	3.53 ± 0.77	4.05 ± 0.89	4.22 ± 0.54
SV-rSkM	2.77 ± 0.53	3.26 ± 0.70	3.37 ± 0.64	3.92 ± 0.43	4.08 ± 0.43*
ESV (ml)					
Control	1.20 ± 0.13	1.49 ± 0.36	1.71 ± 0.34	2.16 ± 0.40	2.34 ± 0.23
WT-rSkM	1.25 ± 0.14	1.28 ± 0.16	1.53 ± 0.37	1.69 ± 0.33	1.88 ± 0.22
SV-rSkM	1.29 ± 0.21	1.39 ± 0.27	1.48 ± 0.25	1.51 ± 0.23*	1.61 ± 0.25**

Abbreviations: EDV, end-diastolic volume; ESV; end-systolic volume; LVIDd, left ventricular dimensions at end diastole; LVIDs, left ventricular dimensions at end systole. Baseline is the time of transplantation, which was 2 weeks after ligation of the left anterior descending coronary artery; other times in weeks are post-transplantation. *$P < 0.05$, **$P < 0.01$ vs. control group at each time point.

and WT-rSkM groups ($P < 0.01$; *Table 2*). The values of the LV chamber diameter/posterior wall thickness were significantly lower in the SV-rSkM group compared with those in the control and WT-rSkM groups ($P < 0.01$; *Table 2*). There were no significant differences between the control and WT-rSkM groups regarding these indices.

The SV-rSkM group exhibited a significantly lower percentage of fibrosis than the control and WT-rSkM groups in the infarcted border area ($P < 0.01$; *Figure 3A*). The diameters of cardiomyocytes in the SV-rSkM group were significantly smaller than those in the control and WT-rSkM groups ($P < 0.01$; *Figure 3B*). There was no significant difference in the area remote from the transplant among the three groups.

3.5 The pro-angiogenic effects of SV

The capillary density 8 weeks after transplantation was significantly higher in the WT-rSkM and SV-rSkM groups than in the control group ($P < 0.01$). Furthermore, the capillary density in the SV-rSkM group was significantly higher than that in the WT-rSkM group ($P < 0.01$; *Figure 3C[a]–C[c]* and *D*). There was no significant difference in the area remote from the transplant among the three groups.

3.6 The accumulation of smooth muscle actin-positive and smooth muscle myosin heavy chain type2-positive cells by SV

Immunohistochemical staining with an anti-SMA antibody revealed that many clusters of SMA-positive cells were present in infarcted areas in the SV-rSkM group (*Figure 3E*). Statistical analysis indicated that the SMA-positive cell density was significantly higher in the WT-rSkM and SV-rSkM groups than in the control group (WT-rSkM , $P < 0.05$; SV-rSkM, $P < 0.01$; *Figure 3F*). Furthermore, the SMA-positive cell density was significantly higher in the SV-rSkM group than in the WT-rSkM group ($P < 0.05$; *Figure 3F*). Notably, SM-MHC type 2-positive cells were also detected in infarcted areas in the SV-rSkM group, whereas those cells were scarce in the control and WT-rSkM groups (*Figure 3G*).

Table 2 Thickness of the infarcted wall and posterior wall and left ventricular chamber diameter

	Control	WT-rSkM	SV-rSkM
Left ventricular chamber diameter (mm)	4.50 ± 0.46	4.48 ± 0.42	3.85 ± 0.29**††
Infarcted wall thickness (mm)	0.53 ± 0.05	0.51 ± 0.08	0.63 ± 0.06
Posterior wall thickness (mm)	2.04 ± 0.10	1.88 ± 0.25	1.96 ± 0.14
Percentage anterior wall thickness	25.98 ± 2.66	27.20 ± 2.63	32.29 ± 0.98**††
Left ventricular chamber diameter/ posterior wall thickness	2.36 ± 0.22	2.30 ± 0.15	1.98 ± 0.16**††

The percentage anterior wall thickness is the infarcted wall thickness/posterior wall thickness × 100. **$P < 0.01$ vs. control group. ††$P < 0.01$ vs. WT-rSkM group.

3.7 The induction of smooth muscle actin by SV

Expression of SMA was increased when SV was added to the isolated fibroblasts (*Figure 4A* and *B*). The expression level of SMA was similar to that of TGF-β1 (*Figure 4B*). Conversely, the expression level of SMA was unchanged by the addition of SV random peptide (*Figure 4A* and *B*).

Downloaded from http://cardiovascres.oxfordjournals.org/ at Osaka University on May 20, 2014

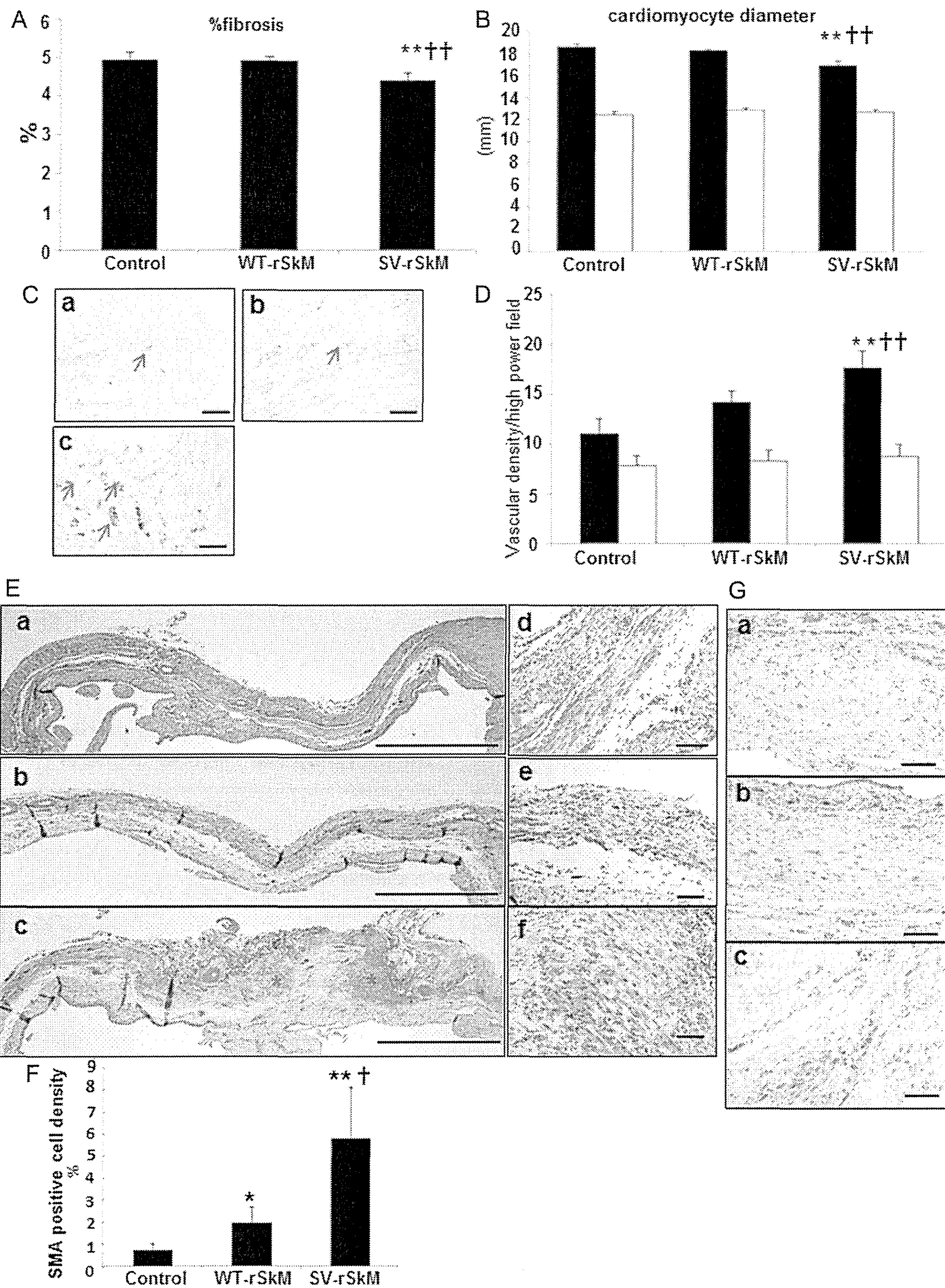

Figure 3 Histological evaluations of LV remodelling. (*A*) Percentage fibrosis. (*B*) Cardiomyocyte diameter. $^{**}P < 0.01$ vs. Control group. $^{††}P < 0.01$ vs. WT-rSkM group. Filled bars, border area; open bars, remote area. Immunohistochemical staining. (*C*) A section of the infarcted border zone stained with an antibody against von Willebrand factor: (*a*) control; (*b*) WT-rSkM; and (*c*) SV-rSkM (×200 magnification, scale bars represent 100 μm). Newly formed vessel is stained brown. (*D*) Quantitative estimation of vascular density. $^{**}P < 0.01$ vs. Control group. $^{††}P < 0.01$ vs. WT-rSkM group. Filled bars, border area; open bars, remote area. (*E*) The distribution of SMA-positive cells: (*a*) control; (*b*) WT-rSkM; (*c*) SV-rSkM (*a–c*, ×20 magnification, scale bars represent 1000 μm; e and *f*, ×200 magnification, scale bars represent 100 μm). Red asterisks denote SMA-positive cells. (*F*) Quantitative estimation of the SMA-positive cell density. $^{*}P < 0.05$, $^{**}P < 0.01$ vs. Control group. $^{†}P < 0.05$ vs. WT-rSkM group. (*G*) The distribution of SM-MHC type 2-positive cells: (*a*) control; (*b*) WT-rSkM; and (*c*) SV-rSkM (*a–c*, ×200 magnification, scale bars represent 100 μm).

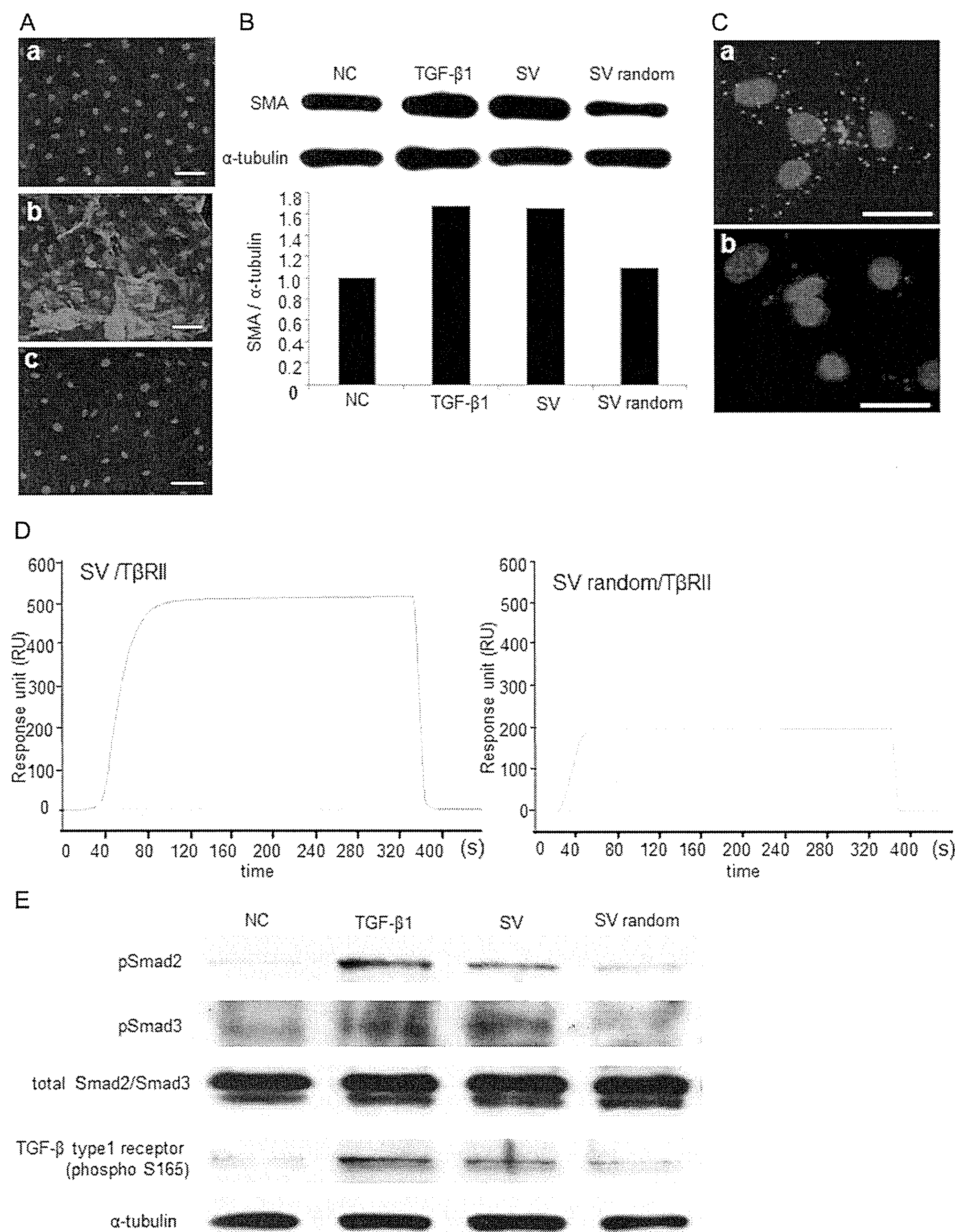

Figure 4 Myofibroblast differentiation induced by exposure of the isolated CFs to SV. (*A*) and (*B*) SMA expression induced by SV. (*A*) Immunofluorescence staining with an anti-SMA antibody: (*a*) non-stimulated CFs (NC); (*b*) CFs exposed to SV; and (*c*) CFs exposed to SV random peptide (×200 magnification, scale bars represent 100 μm). (*B*) Immunoblot of the myofibroblast differentiation marker SMA and its quantitative assessment. α-Tubulin was used as a loading control. (*C*) The examination of binding between TβRII and SV using an *in situ* PLA: (*a*) CFs exposed to SV; (*b*) CFs exposed to SV random peptide (scale bars represent 50 μm). The binding between TβRII and SV and the TGF-β–Smad signalling induced by SV. (*D*) Biacore analysis of the interaction of TβRII with SV. (*E*) Assessment of TGF-β–Smad signalling in CFs exposed to SV by western blotting. α-Tubulin was used as a loading control.

Downloaded from http://cardiovascres.oxfordjournals.org/ at Osaka University on May 20, 2014